

043  
BHA  
12075

ASTROPHYSICAL PROCESSES IN DARK NEBULAE AND  
BINARY SYSTEMS

BY

HARISH CHANDRA BHATT  
PHYSICAL RESEARCH LABORATORY  
AHMEDABAD-380009  
INDIA

A THESIS

SUBMITTED TO THE GUJARAT UNIVERSITY  
FOR THE DEGREE OF

DOCTOR OF PHILOSOPHY

MAY 1983

043

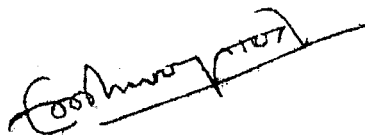


B12075

CERTIFICATE

I hereby declare that the work presented in this thesis is original and has not formed the basis for the award of any degree or diploma by any University or Institution.

Author



HARISH CHANDRA BHATT  
Physical Research Laboratory  
Ahmedabad-380009, India

Certified by



J. N. DESAI  
Professor-in-charge  
Physical Research Laboratory  
Ahmedabad-380009, India

## ABSTRACT

Dark nebulae are dark, dense and cold cosmic clouds of gas and dust that contain a substantial fraction of the total mass of the interstellar medium. It is generally believed that stars are born out of these clouds by some mechanism as yet not fully understood. In some clouds like the Orion Nebula there is ample evidence for current star formation, while the situation for the smaller clouds like the Bok globules is far from clear. This thesis presents the results of a study of some aspects of dark nebulae in general and Bok globules in particular.

With an introduction in Chapter I, we discuss in Chapter II, the frequency distribution of cloud masses, by considering the statistics of dark clouds in our galaxy and also in some extragalactic systems. The existence of power law mass functions for dark clouds is shown, which is consistent with the Oort model for the formation and evolution of interstellar clouds. The mass distribution for clouds in the cloud-complexes is found to be different.

In Chapters III and IV we discuss some physical phenomena that could occur within or in the vicinity of a dark cloud in the galactic environment. In Chapter III we introduce the notion that radiation pressure could drive dust grains from

the interstellar medium into a Bok globule. Consequences of this process are worked out and it is shown that it will result in a dust density distribution in the globule that varies as the inverse cube of the radial distance from the globule centre. This is in excellent agreement with the observations of globules by Schmidt (1975) and Bok (1977). Chapter IV discusses the case of a spherical cloud of gas and dust where the dust grains gravitationally settle towards the centre. It is shown that the segregation of dust grains is size dependent and gives rise to a modification of the grain size distribution in the cloud as a function of time and radial distance from the centre. Expressions are derived for the modified grain size distribution function, average grain size and extinction as functions of distance from the cloud's centre and the age of the cloud. The mean grain size increases towards the centre of the cloud as does the extinction, while in the outer parts of the cloud they both decrease below their normal values. Results of the numerical evaluation of these quantities have been discussed with their implications for the observations of anomalous reddening and polarization within dark clouds and Bok globules.

In Chapter V are presented the results of the polarimetric observations of the Bok globule B 361 carried out in September 1982 in order to study the magnetic field geometry in the globule and to look for the effects of any grain segregation as discussed in Chapter IV. We found that the



magnetic field in the globule is roughly uniform, parallel to the N-S direction and makes an angle about  $45^{\circ}$  to the rotation axis of the globule. The inferred magnetic field strength in the globule is about 50 micro-gauss. The mean dust grain size in the outer parts of the globule is smaller than the normal interstellar grain size. This is consistent with the proposition made in Chapter IV that the larger grains have settled towards the globule centre thus leaving the mean grain size in the outer regions of the globule smaller.

Chapter VI deals with a piece of work on the binary X-ray pulsars. The pulse-period distribution of binary X-ray pulsars has been considered. A gap in this distribution, in the period range  $P \sim 10$  s to  $P \sim 100$  s has been explained in terms of the character of mass transfer in the X-ray binary systems. It is shown that this gap arises because the rotating magnetised neutron stars in these systems are slowed down by accretion torques, either to  $P \lesssim 10$  s when the mass transfer is by mean of Roche-lobe overflow in low mass binaries, or to  $P \gtrsim 100$  s by stellar winds in massive binaries. The gap is maintained as the slow pulsars ( $P > 100$  s) in their spin-up phase cross the gap in a time short compared to their life-time, because of the increase in mass transfer with the evolution of the normal star.

LIST OF PUBLICATIONS

1. The Pulse-period Distribution of Binary X-ray Pulsars,  
Astrophysics and Space Sci., 81, 379 (1982).  
H. C. Bhatt
2. Dust in Bok Globules; in 'Millimeter Wave Astronomy'  
Edited by Beckmann and Phillips, Cambridge University  
Press, (1982), 81.  
I. P. Williams and H. C. Bhatt
3. The Dust Distribution in Bok Globules,  
Mon. Not. Roy. Astr. Soc., 199, 465 (1982).  
I. P. Williams and H. C. Bhatt.
4. Segregation of Dust grains in Dark Clouds,  
Astrophysics and Space Sci., 84, 163 (1982)  
H. C. Bhatt and J. N. Desai
5. Near Infrared photometric Studies of Be stars,  
Bull. D'Information Sur Les Etoiles Be, 6, 19 (1982).  
N. M. Ashok, H. C. Bhatt, P. V. Kulkarni and S. C. Joshi.
6. Optical study of the Solar Corona during the Total Solar  
Eclipse of 16 Feb. 1980,  
Proc. Indian Natn. Sci. Acad., 48A, Suppl. No. 3,  
57 (1982).  
J. N. Desai, T. Chandrasekhar, K. C. Sahu, H. C. Bhatt,  
N. M. Ashok, P. D. Angreji, D. B. Vaidya and V. B. Kamble.

7. Twilight IR Brightening over India due to El Chicho'n  
Volcanic Eruption in Mexico,  
Nature, 300, 620 (1982).  
N.M.Ashok , H.C.Bhatt, T.Chandrasekhar and  
J.N.Desai.
8. Mass Distribution function of dark nebulae,  
To appear in Monthly Not. Roy. Astron. Soc. (1983).  
H.C.Bhatt, D.P.Rowse and I.P.Williams.
9. Polarization Measurements for the Bok Globule B 361,  
Submitted to Monthly Not. Roy. Astron. Soc. (1983).  
I.P.Williams, Karuna VEDI, P.V.Kulkarni,  
H.C.Bhatt, N.M.Ashok , W.K.Griffiths and  
R.E.Wallis.

## ACKNOWLEDGEMENTS

It is a pleasure to express my gratitude to Prof. J.N. Desai, who in addition to providing useful advice, guidance and encouragement, made the work a source of joy and excitement. I would also like to take this opportunity to thank my teachers, collaborators and colleagues working with whom has been a great experience.

Special thanks go to Mr. V. C. Mathew for a neat typing of the manuscript.

Financial support from the Department of Space, Government of India and the British Council is gratefully acknowledged.

# C O N T E N T S

	<u>Page</u>
ABSTRACT	i
LIST OF PUBLICATIONS	iv
ACKNOWLEDGEMENTS	vi
CHAPTER I INTRODUCTION	1
CHAPTER II THE FREQUENCY DISTRIBUTION OF DARK CLOUD MASSES	10
CHAPTER III THE DUST DISTRIBUTION IN BOK GLOBULES	46
CHAPTER IV SEGREGATION OF DUST GRAINS IN DARK CLOUDS	62
CHAPTER V POLARIMETRIC OBSERVATIONS OF THE BOK GLOBULE B 361	81
CHAPTER VI THE PULSE-PERIOD DISTRIBUTION OF BINARY X-RAY PULSARS	95
REFERENCES	111

## CHAPTER I

### INTRODUCTION

The immense space between stars is not empty. It is filled with gas, dust and electromagnetic radiation together with high energy particles and weak interstellar magnetic field. The first evidence for such a pervasive interstellar medium came from observations of interstellar absorption lines (Hartmann, 1904) caused by gas, interstellar extinction (Trumpler, 1930), reddening (Stebbins et al, 1940) and polarization (Hall, 1949 and Hiltner, 1949) caused by dust. More recently observations in radio, microwave, infrared, ultraviolet and X-ray wavelengths have greatly improved our knowledge of the distribution and state of interstellar matter.

The distribution of the components of the interstellar medium is far from uniform. There are thus concentrations of gas and dust; the cosmic clouds or nebulae; that reveal their presence in the interstellar space in a variety of ways, and are known by different names.

#### I.1:1 Dark Nebulae

These are relatively dense clouds of gas and dust often detected optically as dark areas in the midst of rich star fields. They appear dark against a bright background because the dust in these clouds absorbs the light from background stars and

reduces the number of stars seen through the cloud in relation to the density of stars in adjacent areas. The "Coal Sack" near the Southern Cross is one of the most striking examples of a dark cloud visible to the naked eye. The "Great Rift" in the constellation of Cygnus is a result of the overlapping of numerous dark clouds in the galactic equatorial plane.

Dark clouds exhibit a variety of shapes and a large range of sizes. Many smaller dark clouds appear on the telescopic photographs of the Milky Way such as the ones taken by E.E. Barnard at the turn of the century. Some of these dark nebulae of small dimensions, catalogued by Barnard (1927) and also called "Barnard Objects" display compact, quasi-spherical shapes. These compact clouds and the still smaller dark nebulae seen projected against bright nebulosities like M8, are known as "Bok globules" after E. J. Bok who first drew attention to them and suggested that they may represent an early stage of condensation of the interstellar medium leading to the formation of stars (Bok and Reilly, 1947). The most complete catalogue of dark nebulae has been compiled by Lynds (1962) from a study of the Palomar Observatory Sky Survey photographs.

### I. 1:2 Reflection Nebulae

Dusty clouds that become luminous by reflecting the light from a nearby star or some other source of light are called "Reflection nebulae". There are three main types of them. The

'interstellar' reflection nebulae are produced by the illumination of the surrounding interstellar matter by intrinsically luminous stars, as the nebulosity in the Pleiades cluster. The Hubble's variable nebula NGC 2261 is an example of a 'compact' reflection nebula where the dust cloud is more intimately related to the illuminating star, in this case R Mon. The third type of reflection nebulae are the ones that are found at high galactic latitudes and reflect the integrated light of stars in the Galactic disk.

### I.1:3 Emission Nebulae

Emission nebulae are gas clouds that absorb ultra-violet radiation from nearby hot stars and reradiate it in emission lines. The great nebula M42 in Orion is an example visible to the naked eye. Dark dust clouds are often found in the company of such nebulosities. However, the central stars seem to have driven the dust away from their immediate surroundings by means of radiation pressure, stellar wind or some other cause. The hydrogen gas in these nebulae is ionised in a roughly spherical volume around the hot star forming the H II region.

There are other kinds of emission nebulae like the supernova remnants and the planetary nebulae. The high velocity gas expelled in supernova explosions collides with the low density gas of the interstellar medium and produces shocks.



Hydrogen in these shocks is collisionally excited and gives rise to the luminescence observed, for example in the "Loop Nebula". Planetary nebulae such as the "Ring Nebula" in the constellation Lyra appear roughly spherical or ellipsoidal shells of luminous gas, with faint but very hot nuclear stars at the center. They are believed to result from gas ejection from the central stars probably at a late stage of stellar evolution.

#### I. 1:4 Molecular Clouds and H I Clouds

The term 'molecular cloud' is frequently used for the very large clouds in which hydrogen is almost all in the molecular form. The molecular clouds are often associated with the sites of current star formation. There are also less dense clouds of various sizes in which hydrogen is mainly in the atomic form and visual absorption is not large enough for them to be observable as dark clouds. They are called 'H I clouds' or 'Diffuse clouds'.

#### I. 2 Interstellar Clouds and Star Formation

The interstellar medium with its clouds of various kinds is an important structural and dynamical component of the galaxy. It is generally believed, with considerable observational evidence, that stars form out of the interstellar

matter and have their birth place within interstellar clouds of gas and dust, though the details of the star formation process are as yet unclear. And, stars at various stages of evolution throw out matter back to the interstellar medium where again it condenses into clouds. Studies of interstellar clouds are thus of obvious importance for a better understanding of the problems of star formation. Under the diverse environmental conditions and states of matter, interstellar clouds provide a tremendous variety of physical processes and phenomena. By studying the interactions between the gas, dust, radiation, magnetic field, high energy particles and other components of the interstellar medium under different astronomical situations, we may hope to better understand the behaviour, structure and evolution of the interstellar medium and the detailed steps in the star formation process.

### 1.3 Methods of study and Properties of Dark Clouds

A large number of techniques are used to gather information about the objects of our study. Here we briefly review some of the methods of observation and the properties of the dark clouds derived from them. In the optical, the typical methods are the measurement of reddening of background stars and star counts (e.g. Bok and McCarthy, 1974; Schmidt, 1975; Tomita et al., 1979). Reddening is measured by performing multiwavelength photometry, and in the method of star counts

one compares the number of stars per unit area seen through the cloud and in an adjacent area away from the cloud. From these observations one derives the magnitude of extinction caused by the cloud and the amount and distribution of dust in it. Polarization measurements of the background stars also give information about the nature of the dust and the mechanism that aligns the dust grains in the cloud. However, the very dense regions of the dark clouds can not be studied by optical means because of the large absorption in the visual. At longer wavelengths in the infrared, far infrared, microwave and radio one can penetrate deeper into the dark clouds (e.g. Strom et al., 1975; Keene, 1981; Dickman, 1978; Martin and Barrett, 1978; Snell, 1981) and gain knowledge not only about the dust but also the gaseous component of the clouds. Radio observations of a variety of atomic and molecular species (particularly the  $^{13}\text{CO}$  molecule) help us determine the density, temperature and the dynamical properties of these objects. Though the dark nebulae exhibit a range of shapes, sizes and physical properties, the following characteristics may be considered to be typical of an average dark cloud like 'E 361'.

Constituents: Dust and gas. Gas mainly molecular hydrogen  $\text{H}_2$  with traces of  $\text{CO}$ ,  $\text{NH}_3$ ,  $\text{H}_2\text{CO}$ ,  $\text{CS}$ ,  $\text{HCN}$  and others;  $\text{CO}$  being the most abundant after  $\text{H}_2$ . The gas to dust ratio by mass is  $\sim 100$ .

Linear size and Mass:  $R \sim 0.5 \text{ pc}$ ,  $M \sim 50 M_{\odot}$ .

Visual absorption:  $A_v \sim 3 \text{ magnitudes}$ .

Density:  $n(\text{H}_2) \sim 10^3 \text{ cm}^{-3}$ .

Temperature:  $T_{\text{gas}} \sim T_{\text{dust}} \sim 10^0 \text{ K}$ .

Dynamical state: Microwave spectroscopic observations indicate the presence of rotation and suprathermal gas motions in many of the observed dark nebulae (e.g. Martin and Barrett, 1978).

The dust grains in these clouds may be similar to the ones in the intercloud medium in many ways. Thus the grains may be submicron sized solid particles of similar substances as in the normal interstellar medium. Magnetic field  $B$  in the clouds may be of the order of few tens of microgauss ( $\mu\text{G}$ ). We note here that in contrast to the clouds, the intercloud medium is characterized by  $n(\text{H}) \sim 0.3 \text{ cm}^{-3}$ ,  $T \sim 8000 \text{ }^{\circ}\text{K}$  and  $B \sim 3 \mu\text{G}$  (Field, 1973).

#### I.4 Scope of the Present Study

The large molecular clouds and the emission nebulae are generally found together and it seems that active star formation is well under way in them. This is clearly evident in the 'Orion Nebula'. Here one finds hot young stars, H II regions, infrared sources obscured in the visible by dust, dense concentrations of molecular gas emitting strongly in microwave lines, high velocity gas flows and other signs of stellar birth, all side by side. However, the status of the smaller dark nebulae is not clear in this regard. Observations in microwave spectral lines (e.g., Martin and Barrett, 1978) and theoretical arguments based on the 'Virial Theorem' suggest (e.g., Bok, 1977) that most of the observed dark nebulae (Bok globules, Barnard objects and Lynds clouds) are gravitationally bound and perhaps collapsing to give rise to the formation of stars. However, there are no convincing examples of these clouds being in association with new-born stars. In this thesis we focus our attention on these nebulae.

We first make a statistical study of a large sample of these objects to determine the frequency distribution of the cloud masses. The form of the mass spectrum would provide an important constraint on any model for the origin and evolution of the dark clouds. We then consider some general physical processes taking place within and around

an individual dark cloud. These processes involve the motion of dust grains relative to the gas under the forces of gravity, radiation pressure and viscosity; and are discussed with emphasis on their relevance to the observed phenomena in dark nebulae. Effects of radiation pressure driving dust grains into dark globules and gravitational settling of dust have been investigated. Polarimetric observations of the Bok globule 'B 361' are presented. These observations were carried out to find the magnetic field geometry in the globule and to look for the effects of dust segregation discussed in this thesis. Implications of the results of these investigations have also been discussed.

## CHAPTER II

### THE FREQUENCY DISTRIBUTION OF DARK CLOUD MASSES

When the members of a population of astronomical objects display a large range in any of their physical properties, a statistical analysis may be expected to provide some clues as to the nature of the physical processes responsible for their formation and subsequent evolution. Stars in our galaxy show a mass spectrum with a preponderance of low mass stars. Salpeter (1955) obtained an empirical relationship between the number of stars per unit mass range  $N(M)$  and the mass  $M$  in the form of a power law

$$N(M) \propto M^{-s}$$

and found the power index 's' to be 2.35. There have been many attempts (e.g. Kushwaha and Kothari, 1960; Fowler and Hoyle, 1963; Reddish, 1978; Bhattacharjee and Williams, 1980) to derive the stellar mass distribution with various assumptions about the star formation process.

Now, the interstellar clouds come in all sizes and states of condensation and it is widely believed that stars form from these clouds by gravitational collapse. If stars formed

by a simple gravitational contraction of interstellar clouds, it would be natural to expect the frequency distributions of the masses of stars and of the clouds to be related. In any case it is of considerable interest to perform a statistical study to find out the nature of the distribution of cloud masses. In particular it would be interesting to see whether the clouds also follow a power law mass distribution function and if they do, how does it compare with that for stars and other astronomical objects. The form of the mass function for clouds would provide an important constraint for the theory of their formation, evolution and their connection with stars. In this chapter we present and discuss the results of such a study of the mass distribution of dark clouds in our galaxy, the Andromeda galaxy and the Magellanic Clouds.

## II. 1 Catalogues of Dark Nebulae

Dark nebulae are a fairly common feature of our galaxy. Some are isolated identities while others can be found in complexes such as the 'Orion' or the 'Southern Coalsack'. There are many catalogues of the galactic dark nebulae (e.g. Lundmark and Melotte, 1926; Barnard, 1927; Khavtassi, 1960; Lynds, 1962; Schoenberg, 1964). The most uniform and complete catalogue is the one prepared by Lynds (1962) from the Palomar Observatory Sky Survey photographs. We use this catalogue for our study of the galactic **dark** clouds. The catalogue gives positions (co-ordinates), angular area



in square degrees and opacity on a scale from 1 to 6 for each of the 1802 nebulae. Star counts are used to identify the clouds and to estimate their opacity. The opacity estimates are approximately equivalent to the extinction  $A_v$ .

Hodge has catalogued the dark nebulae in the Andromeda galaxy M31 (Hodge, 1980), the Large Magellanic Cloud (Hodge, 1972) and the Small Magellanic Cloud (Hodge, 1974). These catalogues contain 730, 68 and 45 clouds respectively. The positions, dimensions and in the case of the nebulae in the Magellanic Clouds the opacity estimates are given.

## II.2 Completeness of the Catalogues

A dark nebula is observed when there is an appreciable reduction in the number of stars seen through a cloud caused by absorption. Therefore the detectability of dark nebulae depends on:

1. The magnitude of absorption caused by the dust in the cloud.
2. The size of the cloud.
3. The density of background stars.
4. The density of foreground stars.

Thus, very tenuous clouds with  $A_v \ll 1$  and very small clouds whose dimensions are less than or of the order of the mean spacing of stars tend to be missed. For the galactic clouds, the minimum detectable size increases rapidly with increasing latitude because the stellar background becomes too thin. Very distant clouds are difficult to detect because of the increasing number of foreground stars. The minimum detectable cloud size for clouds in the Andromeda galaxy and the Magellanic Clouds is much larger because of their large distance and the existence of a limiting angular resolution inherent to the method of cloud detection. We will discuss the observed distribution of cloud masses taking these effects into account.

### II.3 The Mass of the Clouds and the Mass Function

If the distance  $D$  to a cloud is known, its angular area  $A_1$ , given in the catalogue, can be converted into a real cross section  $S$  using  $S = A_1 D^2$ . The opacity  $A_2$  of the cloud is related to the column density of absorbing matter (dust mixed with gas) along the line of sight through the cloud. We use the conversion formula (e.g. Jenkins and Savage, 1974) :

$$N(H) = 2.5 \times 10^{21} A_2 \text{ cm}^{-2},$$

where  $N(H)$  is the number of hydrogen atoms per unit area

along the line of sight and  $A_2$  is measured in magnitudes.

The mass  $M$  of the cloud is then given by  $S N(H) m_H$ , where  $m_H$  is the mass of a hydrogen atom. We obtain for the mass of the cloud in units of the solar mass  $M_\odot$  :

$$\left( \frac{M}{M_\odot} \right) = 62.5 \left( \frac{A_1}{\text{square degrees}} \right) \left( \frac{A_2}{\text{magnitudes}} \right) \left( \frac{D}{100 \text{ pc}} \right)^2$$

The distances to the clouds in the Andromeda galaxy ( $D = 670$  kpc), the Large Magellanic Cloud (55 kpc) and the Small Magellanic Cloud (63 kpc) are known. For the galactic clouds the distances are in general not known. There are, however, some cloud complexes in which all the member clouds can be considered to be roughly at the same distance and the distances to the complexes are known. From the Lynds catalogue we identify, following Rowan-Robinson (1979), three cloud complexes, namely Orion (500 pc),  $\rho$  Ophiuchi (170 pc) and Taurus (100 pc). For the rest of the clouds we make various assumptions regarding their distances as will be discussed later.

Having evaluated the cloud masses it is easy to determine their frequency distribution. The whole range of masses is divided into a number of bins and the number of clouds in the different mass bins counted. Since the

range of masses is very large we have made logarithmic mass bins. The number of bins is decided on the basis of both the mass range and the total number of clouds in the sample. The results on the frequency distribution of cloud masses are presented in the form of Tables giving the number of clouds in different mass bins.

The mass distribution function  $N(M)$  for the clouds is defined (e.g. Penston et al., 1969) to be the number of clouds per unit mass range so that  $N(M) dM$  gives the number of clouds with masses between  $M$  and  $M+dM$ .  $N(M)$  can be easily calculated from the data on the frequency distribution given in the Tables.  $\log N(M)$  is then plotted against  $\log M$ . For a distribution function of the form  $N(M) \propto M^{-s}$ , such a plot would be a straight line of slope ' $-s$ '.  $\log N$  vs  $\log M$  plots are displayed in the Figures. The error bars represent the expected statistical fluctuations in the number of clouds in different mass bins. Our treatment of the errors is similar to that by Penston et al. (1969). The error involved in calculating an individual cloud mass, given the correctness of the assumption regarding the distance arises from errors in angular area and opacity. The error in measuring angular area is about 1%, while the maximum error in opacity is 1/2 magnitude in an average measurement of 3 or 4 magnitudes. The total error is thus less than a factor of 1/6, while the width of the mass bins used is generally a factor of about 3 or more. Thus the probability that an individual

cloud is placed in the wrong mass bin is small. Since the arguments have to be made a large number of times the errors can be statistically modelled using Poisson statistics. We therefore assume that the probable error in the number of clouds  $n$  in each mass bin is  $\sqrt{n}$  and the ensuing error bars are shown in the diagrams. We have determined the values of the index 's' for the various cases we consider by fitting least square straight lines to the linear portions of the Log N - Log M plots.

#### II.4 Results

Tables II.1 through II.9 and Figures II.1 through II.9 give the results obtained for the various cloud populations. The Tables contain the number of clouds in different mass bins, the mean cloud mass  $M$  for the bin and the mass function  $N(M)$ . Plots of Log  $N(M)$  against Log  $M$  are presented in the Figures. The least square straight line fits to the linear portions have been indicated. The index 's' and the correlation coefficient 'r' of the straight line fit have been calculated and given in the Tables.

##### II.4:1 Results for the Cloud Complexes

There are three prominent complexes of clouds at relatively large galactic latitudes. There is of course no absolute test for clouds belonging to a complex. We shall

assume that clouds whose positions are close to each other in the sky (especially at large galactic latitudes) form a complex, and in particular we follow Rowan-Robinson (1979) in defining membership of the three complexes Orion,  $\rho$  Ophiuchi and Taurus as follows.

All clouds with position in the range  $5^{\text{h}}24^{\text{m}} < \alpha < 6^{\text{h}}12^{\text{m}}$ ,  $-10^{\circ} < \delta < 4^{\circ}$  were defined to belong to the Orion complex ( $D = 500$  pc) while the  $\rho$  Ophiuchi complex ( $D = 170$  pc) is defined by  $16^{\text{h}}14^{\text{m}} < \alpha < 16^{\text{h}}38^{\text{m}}$ ,  $-25^{\circ}40' < \delta < -21^{\circ}40'$  and the Taurus complex ( $D = 100$  pc) as  $4^{\text{h}} < \alpha < 5^{\text{h}}$ ,  $22^{\circ} < \delta < 32^{\circ}$ . The exact numerical value for the distance is not important as it acts only as a scaling factor. What is important is the assumption of equal distance for the clouds in a complex. With this assumption regarding distance, it is possible to follow through the procedure outlined in Section II.3 and produce the frequency distribution of cloud masses and the mass function for each of the three complexes. These are shown in the Tables II.1 through II.3 and the Figures II.1 through II.3.

It is immediately evident that the mass distribution for the Orion complex (Fig. II.1) and the  $\rho$  Ophiuchi complex (Fig. II.2) are very similar and that a very good straight line can be fitted to the data. For Orion, the best fit line, using the method of least square fitting, has a slope of -0.95. For  $\rho$  Ophiuchi, the best fit line has a slope of -0.98. The

Table II.1  
The Orion Complex

<u>The Mass Bins</u>				<u>The Frequency Distribution</u>	
Bin	Min. Mass ( $M/M_{\odot}$ )	Max. Mass ( $M/M_{\odot}$ )	Mean Mass ( $M/M_{\odot}$ )	Number of clouds	Mass Function $N(M/M_{\odot})$
1	1.88 E+1	8.65 E+1	5.26 E+1	4	5.89 E-2
2	8.65 E+1	3.99 E+2	2.43 E+2	6	1.92 E-2
3	3.99 E+2	1.84 E+3	1.12 E+3	7	4.85 E-3
4	1.84 E+3	8.50 E+3	5.17 E+3	4	6.01 E-4
5	8.50 E+3	3.92 E+4	2.38 E+4	7	2.28 E-4

Power law index 's' = 0.953

Correlation coefficient 'r' = 0.993

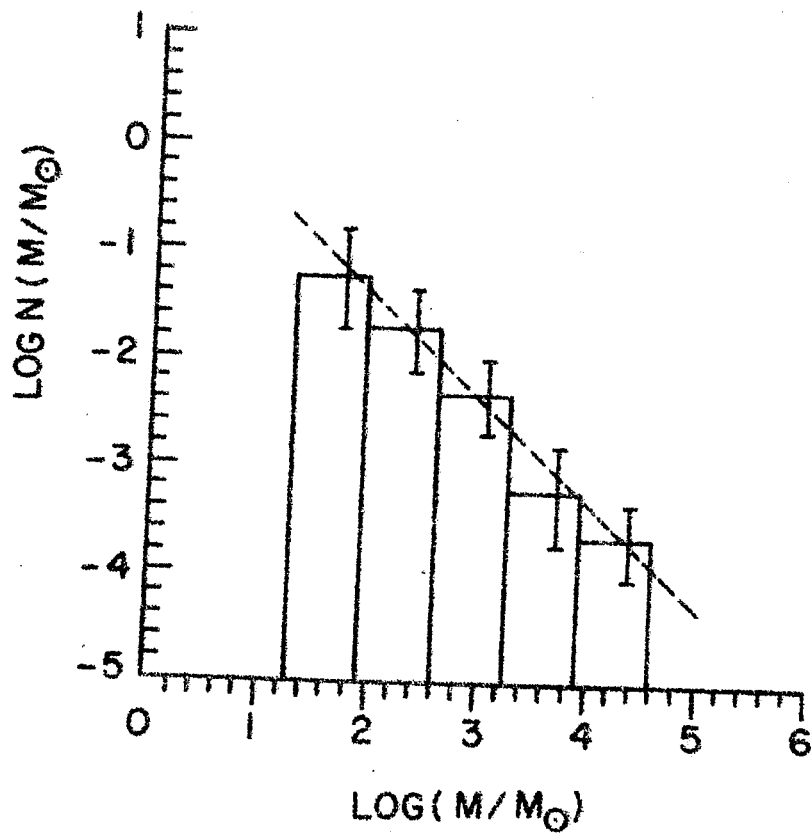


Figure II.1 : Mass distribution function for the clouds in the Orion complex. The broken line is the least square fit.  $s = 0.953$ ,  $r = 0.993$ .



Table II.2  
The  $\rho$  Ophiuchi Complex

Bin	The Mass Bins			The Frequency Distribution	
	Min. Mass ( $M/M_{\odot}$ )	Max. Mass ( $M/M_{\odot}$ )	Mean Mass ( $M/M_{\odot}$ )	Number of clouds	Mass Function ( $N(M/M_{\odot})$ )
1	6.30 E+0	2.01 E+1	1.32 E+1	7	5.09 E-1
2	2.01 E+1	6.38 E+1	4.20 E+1	3	6.85 E-2
3	6.38 E+1	2.03 E+2	1.34 E+2	6	4.31 E-2
4	2.03 E+2	6.47 E+2	4.25 E+2	4	9.02 E-3
5	6.47 E+2	2.06 E+3	1.35 E+3	7	4.95 E-3

Power law index 's' = 0.975

Correlation coefficient 'r' = 0.979

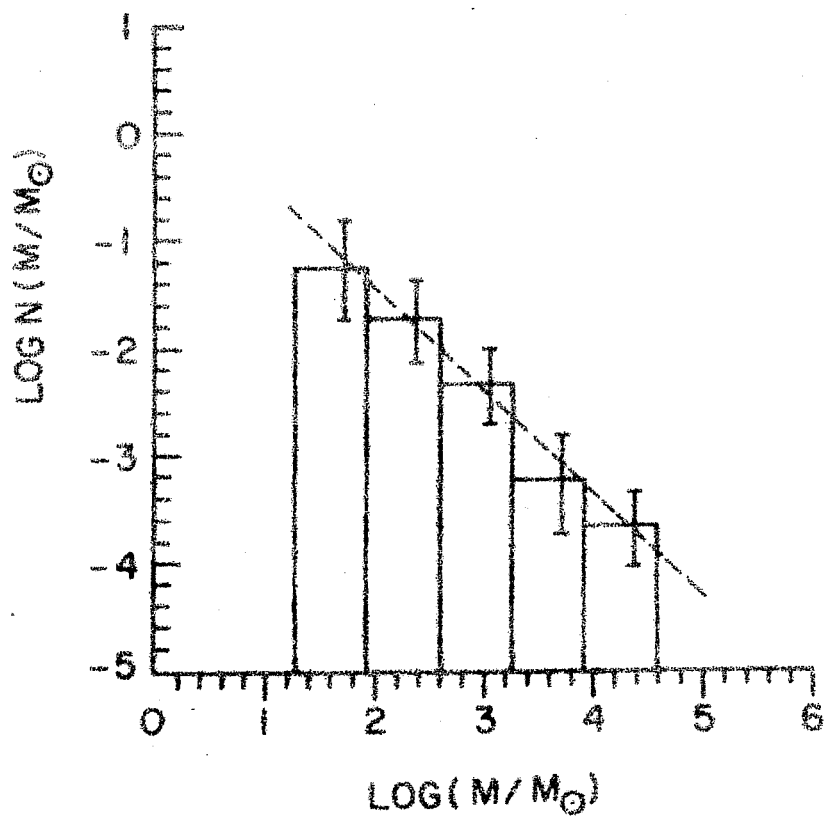


Figure II.2 : Mass distribution function for the clouds in the  $\rho$  Ophiuchi complex. The broken line is the least square fit.  $s = 0.975$ ,  $r = 0.979$ .

Table II.3

The Taurus Complex

Bin	The Mass Bins			The Frequency Distribution	
	Min. Mass ( $M/M_{\odot}$ )	Max. Mass ( $M/M_{\odot}$ )	Mean Mass ( $M/M_{\odot}$ )	Number of Clouds	Mass Function $N(M/M_{\odot})$
1	1.25 E+0	3.26 E+0	2.26 E+0	3	1.49 E+0
2	3.26 E+0	8.50 E+0	5.88 E+0	3	5.72 E-1
3	8.50 E+0	2.22 E+1	1.53 E+1	7	5.12 E-1
4	2.22 E+1	5.78 E+1	4.00 E+1	11	3.08 E-1
5	5.78 E+1	1.51 E+2	1.04 E+2	10	1.08 E-1
6	1.51 E+2	3.93 E+2	2.72 E+2	5	2.06 E-2
7	3.93 E+2	1.03 E+3	7.09 E+2	3	4.75 E-3

(a) Using all mass bins:

Power law index 's' = 0.948

Correlation coefficient 'r' = 0.961

(b) Ignoring the first three mass bins:

Power law index 's' = 1.479

Correlation coefficient 'r' = 0.996

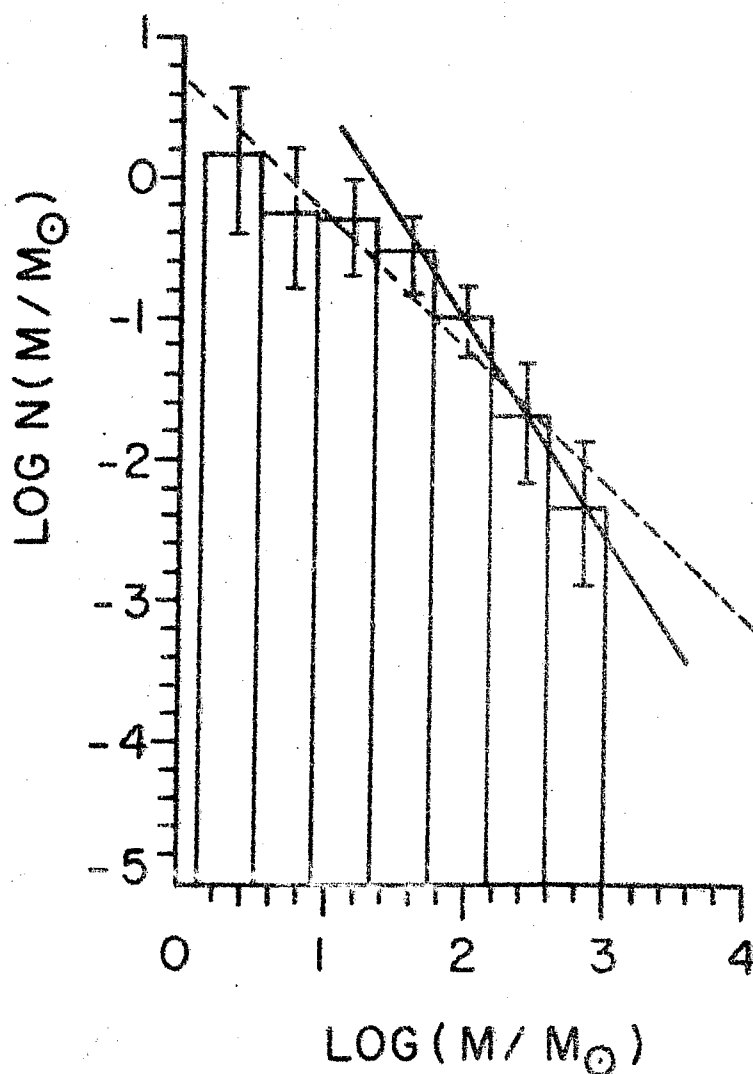


Figure II.3 : Mass distribution function for the clouds in the Taurus complex. The broken line is the least square fit to all the points whereas the fit ignoring the three lowest mass points is indicated by the solid line.

$s = 0.948, \quad r = 0.961$  (broken line).

$s = 1.479, \quad r = 0.996$  (solid line).

correlation coefficients for the straight line fit for the two complexes are 0.993 and 0.979 respectively. We note here that the values of the slope ( $-s$ ) for the Orion and  $\rho$  Ophiuchi complexes are very close to -1 and indicate equal number of clouds in equal logarithmic mass intervals. These results agree well with the analysis of Rowan-Robinson (1979) who investigated the number/radius relationship for clouds in these complexes.

The results for the Taurus complex (Table II.3, Figure II.3) are somewhat different in that no good straight line fit appears possible. The least square single straight line fit to all the points has a slope -0.95, while in view of the possibility of missing low mass clouds, the best fit line on ignoring the three low mass points has a slope -1.48. More discussion on the Taurus complex will be given later.

#### II.4:2 The Remaining Galactic Clouds

The total number of clouds included in the three complexes is 97. Thus the vast majority of the clouds in the Lynds catalogue have not been analysed. The problem with these clouds of course is that their distances are not known. In what follows we propose three different models which give the cloud distances and we shall determine the mass distribution of the clouds according to each model. The first two models are the two extremes of possible models,

as far as the effect of distance on the mass distribution is concerned, while the third is a stochastic model. The three models we consider and the results on the mass distribution are as follows.

Model (a):

It is assumed that all the clouds are at the same distance from us. In view of the fact that the star count method can not be effective in detecting clouds at large distances (say,  $D > 600$  pc) because of the increasing number of foreground stars and that the volume containing the clouds increases as the cube of the distance from us, most of the detected clouds will be at some average distance from us (say, 400 pc). Thus this model with the assumption of constant distance of the clouds may be reasonably realistic.

The resulting distribution of cloud masses and the mass function for this model are shown in Table II.4 and Figure II.4 respectively. From Figure II.4 it is evident that a straight line is a poor representation over the whole range of masses while a straight line is in fact a very good fit if the three lowest mass points are ignored. The least square fit gives a slope for this line of -1.53 with a correlation coefficient equal to 0.996.

Table II. 4  
The Galactic Clouds : Model (a)

Bin	The Mass Bins			The Frequency Distribution	
	Min. Mass ( $M/M_{\odot}$ )	Max. Mass ( $M/M_{\odot}$ )	Mean Mass ( $M/M_{\odot}$ )	Number of Clouds	Mass Function $N(M/M_{\odot})$
1	3.00 E+0	8.76 E+0	5.88 E+0	66	1.15 E+1
2	8.76 E+0	2.56 E+1	1.72 E+1	207	1.23 E+1
3	2.56 E+1	7.47 E+1	5.01 E+1	328	6.68 E+0
4	7.47 E+1	2.18 E+2	1.46 E+2	361	2.52 E+0
5	2.18 E+2	6.36 E+2	4.27 E+2	289	6.91 E-1
6	6.36 E+2	1.86 E+3	1.25 E+3	205	1.68 E-1
7	1.86 E+3	5.43 E+3	3.64 E+3	141	3.95 E-2
8	5.43 E+3	1.58 E+4	1.06 E+4	65	6.24 E-3
9	1.58 E+4	4.62 E+4	3.10 E+4	20	6.58 E-4
10	4.62 E+4	1.35 E+5	9.06 E+4	15	1.69 E-4

Power law index 's' = 1.534

Correlation Coefficient 'r' = 0.996

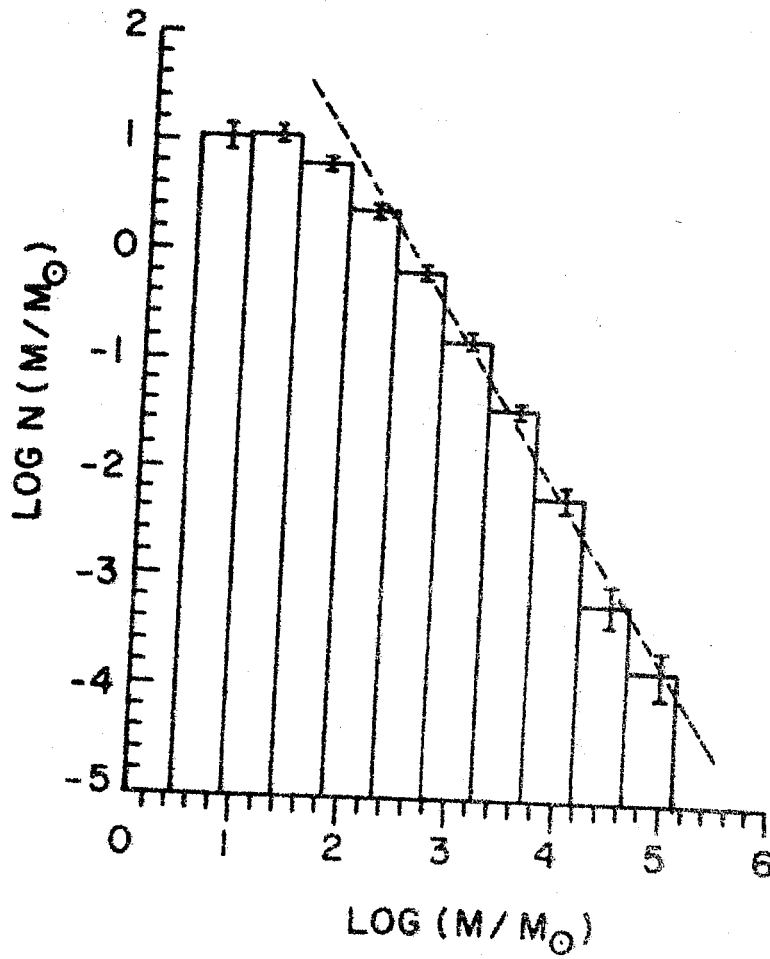


Figure II.4 : Mass distribution function for the galactic clouds. Model (a). The least square fit to the higher mass points is indicated by the broken line.

$$s = 1.534, \quad r = 0.996.$$



Model (b):

For this case we consider a model which is as extreme from model (a) as possible. Here we assume that clouds are homogeneously distributed in space, so that if  $N(D) dD$  is the number of clouds with distances between  $D$  and  $D + dD$ , then

$$N(D) dD = 4\pi K D^2 dD ,$$

$K$  being a constant. All the observed clouds are distributed in space between  $D = 0$  pc and  $D = 600$  pc from us and clouds which appear to have the largest angular cross-section are nearest us while those with the smallest angular size are farthest away. The Lynds catalogue was thus reordered in order of decreasing angular size and increasing distances assigned to the clouds. The space was divided into sub-volumes (spherical shells with radii 0-60, 60-120, . . . . ., 540-600 pc) and the number of clouds in each such volume calculated. Each such cloud was assigned the mean distance of the sub-volume and the actual clouds assigned to the sub-volumes in order from the rearranged catalogue. The cloud masses are then calculated. The resulting frequency distribution of cloud masses and the mass function are shown in Table II.5 and Figure II.5 respectively.

The results from model (b) are similar to the

Table II.5

The Galactic Clouds : Model (b)

Bin	The Mass Bins			The Frequency Distribution	
	Min. Mass ( $M/M_{\odot}$ )	Max. Mass ( $M/M_{\odot}$ )	Mean Mass ( $M/M_{\odot}$ )	Number of Clouds	Mass Function $N(M/M_{\odot})$
1	6.11 E+0	1.28 E+1	9.47 E+0	58	8.64 E+0
2	1.28 E+1	2.69 E+1	1.99 E+1	76	5.40 E+0
3	2.69 E+1	5.64 E+1	4.17 E+1	159	5.39 E+0
4	5.64 E+1	1.18 E+2	8.74 E+1	309	4.99 E+0
5	1.18 E+2	2.48 E+2	1.83 E+2	321	2.47 E+0
6	2.48 E+2	5.21 E+2	3.84 E+2	264	9.69 E-1
7	5.21 E+2	1.09 E+3	8.06 E+2	275	4.82 E-1
8	1.09 E+3	2.29 E+3	1.69 E+3	151	1.26 E-1
9	2.29 E+3	4.80 E+3	3.55 E+3	72	2.87 E-2
10	4.80 E+3	1.01 E+4	7.44 E+3	12	2.28 E-3

Power law index 's' = 1.641

Correlation coefficient 'r' = 0.973

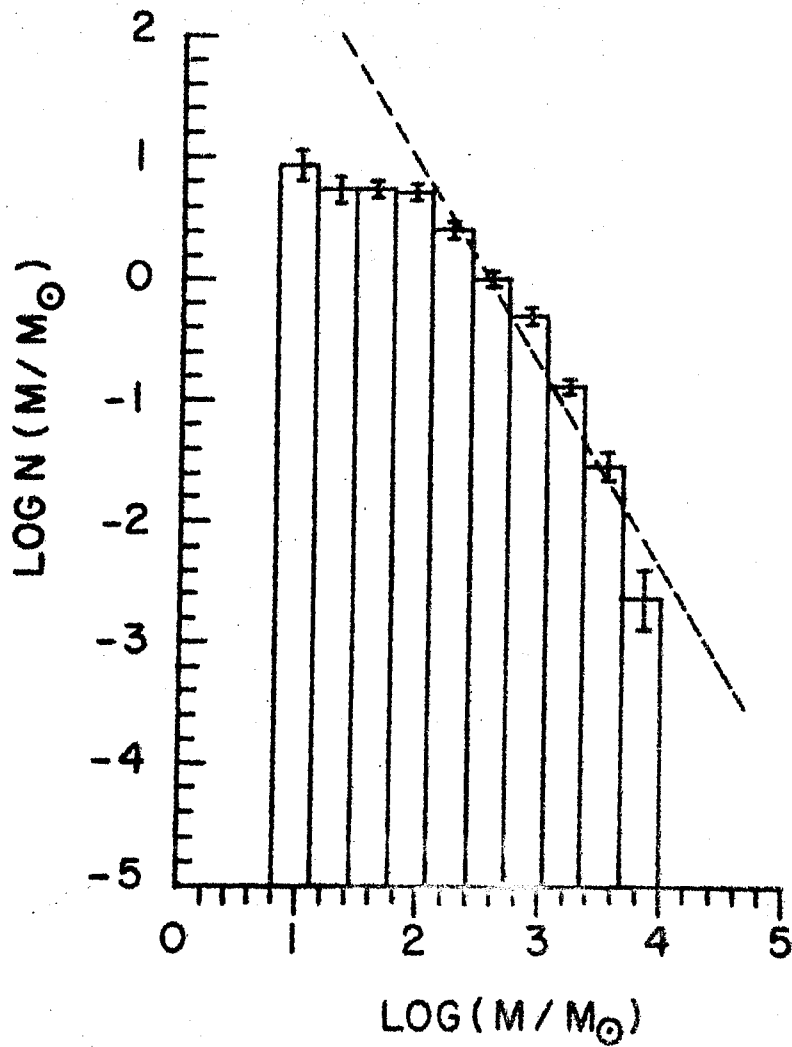


Figure II.5 : Mass distribution function for the galactic clouds. Model (b). The least square fit to the higher mass points is indicated by the broken line.

$$s = 1.641, \quad r = 0.973.$$

results from model (a). In Figure II.5 a straight line fit over the whole mass range is not very good, while a good straight line fit is obtained on ignoring the three lowest mass points. The least square fit to the latter data has a slope of  $-1.64$  with a correlation coefficient  $0.973$ .

#### Model (c):

Models were produced where the clouds are again homogeneously distributed in space between  $D = 0$  pc and  $D = 600$  pc, so that the number of clouds in each sub-volume is known. However, in these models the clouds were assigned to each sub-volume using a random number generator. That is, the required number of clouds in a sub-volume is picked up from the catalogue randomly. In total, five such models were generated, each using a different set of random numbers. The results on the mass distribution and the mass function from all five models are so very similar that we show only one of them in Table II. 6 and Figure II. 6.

Again, the flattening at the lower mass end is present and on ignoring the four lowest mass points the least square straight line fit for the mass function from these five models has slopes  $-1.49$  (shown in Table II. 6 and Figure II. 6),  $-1.50$ ,  $-1.44$ ,  $-1.45$  and  $-1.55$  with correlation coefficients  $0.996$ ,  $0.996$ ,  $0.997$ ,  $0.997$  and  $0.997$

Table II.6

The Galactic Clouds : Model (c) 1

Bin	The Mass Bins			The Frequency Distribution	
	Min.	Max.	Mean	Number	Mass
	Mass ( $M/M_{\odot}$ )	Mass ( $M/M_{\odot}$ )	Mass ( $M/M_{\odot}$ )	of Clouds	Function $N(M/M_{\odot})$
1	2.91 E-1	1.09 E+0	6.88 E-1	6	7.55 E+0
2	1.09 E+0	4.05 E+0	2.57 E+0	15	5.06 E+0
3	4.05 E+0	1.51 E+1	9.59 E+0	121	1.09 E+1
4	1.51 E+1	5.65 E+1	3.58 E+1	328	7.94 E+0
5	5.65 E+1	2.11 E+2	1.34 E+2	447	2.90 E+0
6	2.11 E+2	7.87 E+2	4.99 E+2	328	5.69 E-1
7	7.87 E+2	2.94 E+3	1.86 E+3	247	1.15 E-1
8	2.94 E+3	1.10 E+4	6.95 E+3	142	1.77 E-2
9	1.10 E+4	4.09 E+4	2.60 E+4	46	1.54 E-3
10	4.09 E+4	1.53 E+5	9.69 E+4	17	1.52 E-4

Power law index 's' = 1.494

Correlation coefficient 'r' = 0.996

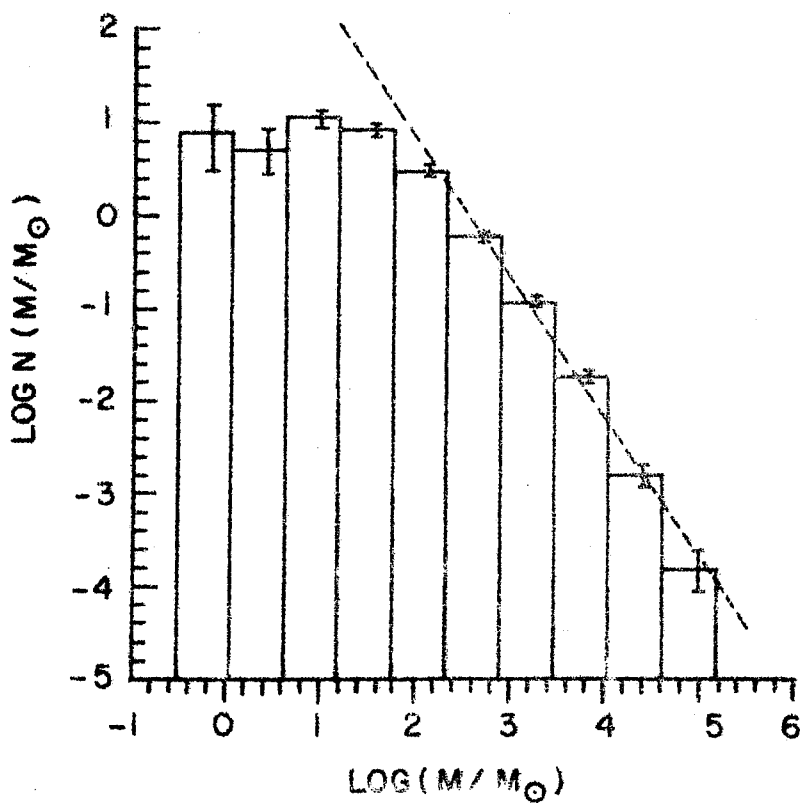


Figure II. 6 : Mass distribution function for the galactic clouds.  
 Model (c). The least square fit to the higher mass  
 points is indicated by the broken line.  
 $s = 1.494$ ,  $r = 0.996$ .

respectively. The mean value of the slope for the five runs is  $-1.49$  with a standard deviation of  $0.04$ . We note here that models (c) give results similar to model (a) because most clouds tend to lie in a narrow range of distances around  $400$  pc even though they are picked up randomly from the catalogue.

#### II. 4:3 Clouds in the Andromeda Galaxy

The catalogue of dark nebulae in the Andromeda galaxy (M31) by Hodge (1980) gives their dimensions, but no opacity estimates are made. However, if the M31 clouds are similar to the large galactic clouds they would display a very small range in the opacity. We assume that all the clouds have the same opacity and that is 2 magnitudes. The product of the linear dimensions given in the catalogue is taken to represent the angular area of the cloud. With these assumptions it is possible to estimate the cloud masses following the procedure outlined in section II. 3. The results are shown in Table II. 7 and Figure II. 7. The least square straight line fit to the mass function plot (Figure II. 7) ignoring the two lowest mass points has a slope of  $-1.73$  with a correlation coefficient  $0.999$ .

#### II. 4:4 Nebulae in the Magellanic Clouds

The catalogues of dark nebulae in the Large Magellanic Cloud (LMC) and the small Magellanic Cloud (SMC)

Table II.7  
Clouds of the Andromeda Galaxy

Bin	The Mass Bins			The Frequency Distribution	
	Min.	Max.	Mean	Number of clouds	Mass
	Mass ( $M/M_{\odot}$ )	Mass ( $M/M_{\odot}$ )	Mass ( $M/M_{\odot}$ )		Function $N(M/M_{\odot})$
1	1.60 E+4	4.47 E+4	3.04 E+4	18	6.27 E-4
2	4.47 E+4	1.25 E+5	8.48 E+4	102	1.27 E-3
3	1.25 E+5	3.49 E+5	2.37 E+5	293	1.31 E-3
4	3.49 E+5	9.76 E+5	6.63 E+5	194	3.09 E-4
5	9.76 E+5	2.73 E+6	1.85 E+6	75	4.28 E-5
6	2.73 E+6	7.63 E+6	5.18 E+6	31	6.33 E-6
7	7.63 E+6	2.13 E+7	1.45 E+7	17	1.24 E-6

---

Power law index 's' = 1.733

Correlation coefficient 'r' = 0.999



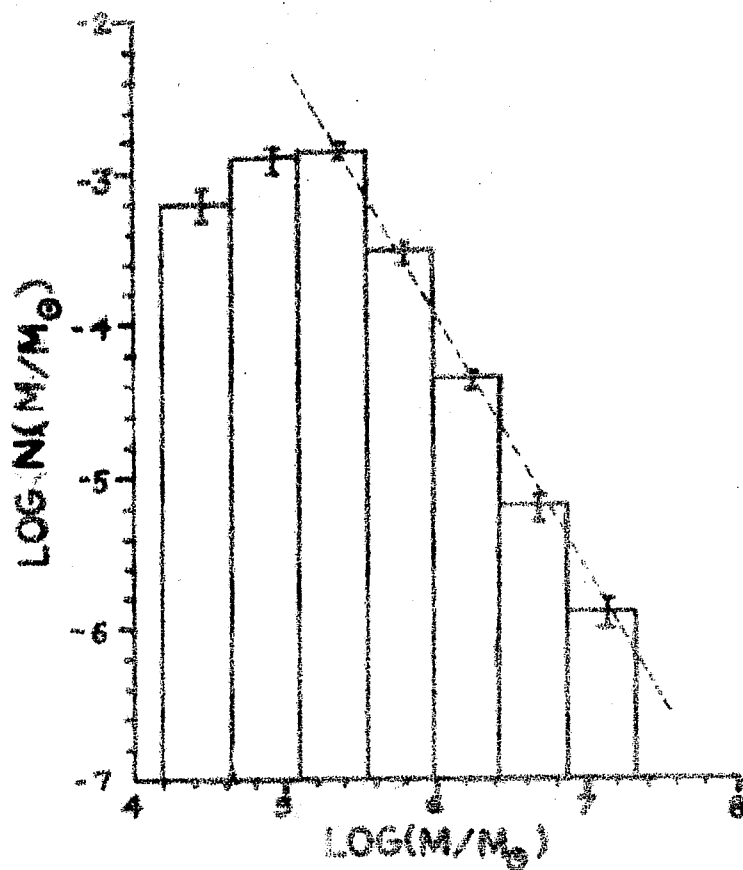


Figure II.7 : Mass distribution function for the clouds in the Andromeda galaxy. The least square fit to the higher mass points is indicated by the broken line.

$$s = 1.733, \quad r = 0.999.$$

by Hodge (1972, 1974) were used to find the mass distributions. The results are shown in Tables II. 8 and II.9 and Figures II. 8 and II.9. In Figure II. 8 for the LMC clouds, the least square straight line fit ignoring the two lowest mass points, has a slope of  $-1.63$  with a correlation coefficient  $0.999$ . For the SMC clouds the range of masses is very small. The mass function plot is shown in Figure II.9. In this case fitting any straight line to the data would not be of much significance.

The results on the mass distributions for the different cloud-sets are summarized in Table II.10, which gives the numerical data regarding the least square fit for each case.

## II.5 Discussion and Conclusions

For the galactic clouds (excluding the clouds belonging to the complexes), despite making rather different assumptions regarding their distances, all models gave very similar results on the frequency distribution of masses and the mass function. Clouds in M31 and the LMC also show similar distributions. In all cases the plots of mass function show a flattening towards the low mass end, and this we attribute to the observational difficulty of detecting the small clouds. However, the points for the higher mass ranges can all be fitted to a high degree of accuracy with a straight line indicating a power law mass function. The slope of the

Table II.8  
Clouds of the LMC

Bin	The Mass Bins			The Frequency Distribution	
	Min. Mass ( $M/M_{\odot}$ )	Max. Mass ( $M/M_{\odot}$ )	Mean Mass ( $M/M_{\odot}$ )	Number of Clouds	Mass Function $N(M/M_{\odot})$
1	1.05 E+4	2.43 E+4	1.74 E+4	6	4.35 E-4
2	2.43 E+4	5.62 E+4	4.02 E+4	11	3.45 E-4
3	5.62 E+4	1.30 E+5	9.30 E+4	24	3.26 E-4
4	1.30 E+5	3.00 E+5	2.15 E+5	14	8.21 E-5
5	3.00 E+5	6.95 E+5	4.98 E+5	8	2.03 E-5
6	6.95 E+5	1.61 E+6	1.15 E+6	5	5.48 E-6

Power law index 's' = 1.628

Correlation coefficient 'r' = 0.999

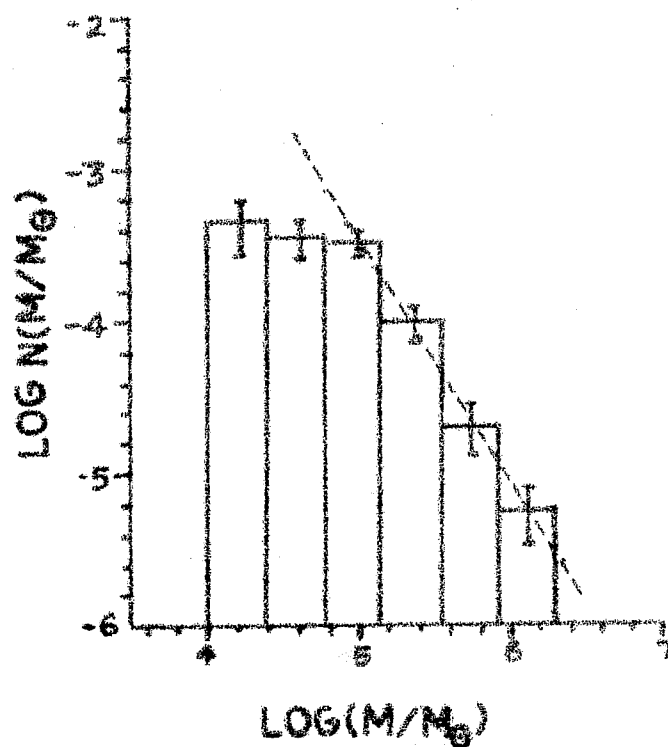


Figure 11.8 : Mass distribution function for the clouds in the LMC. The least square fit to the higher mass points is indicated by the broken line.

$$s = 1.628, \quad r = 0.999.$$

Table II.9  
Clouds of SMC

Bin	The Mass Bins			The Frequency Distribution	
	Min. Mass ( $M/M_{\odot}$ )	Max. Mass ( $M/M_{\odot}$ )	Mean Mass ( $M/M_{\odot}$ )	Number of Clouds	Mass Function $N(M/M_{\odot})$
1	2.07 E+4	4.14 E+4	3.10 E+4	8	3.86 E-4
2	4.14 E+4	8.28 E+4	6.21 E+4	22	5.31 E-4
3	8.28 E+4	1.66 E+5	1.24 E+5	15	1.81 E-4

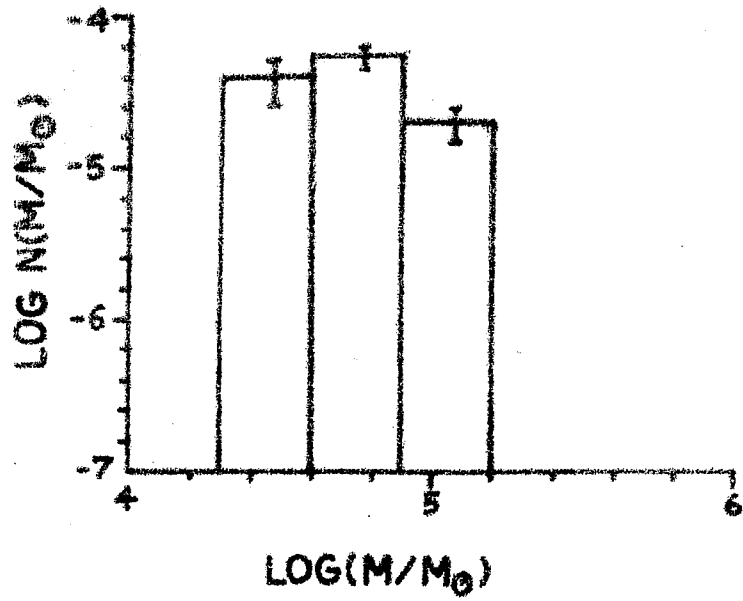


Figure II.9 : Mass distribution function for the clouds in the SMC.

Table II. 10

Results on the Mass Distribution of Clouds : Data Regarding the Least Square Fit.

Cloud set	Number of Clouds	Least square fit value of the index 's'	Correla- tion coeffi- cient 'r'	Number of low mass bins ignored
<u>The Cloud Complexes:</u>				
Orion	28	0.953	0.993	0
♌ Ophiuchi	27	0.975	0.979	0
Taurus	42	0.948	0.961	0
Taurus	42	1.479	0.996	3
<u>The Galactic Clouds:</u>				
Model (a)	1697	1.534	0.996	3
Model (b)	1697	1.641	0.973	3
Model (c) 1	1697	1.494	0.996	4
Model (c) 2	1697	1.499	0.996	4
Model (c) 3	1697	1.444	0.997	4
Model (c) 4	1697	1.453	0.997	4
Model (c) 5	1697	1.553	0.997	4
<u>The Extragalactic Clouds:</u>				
Andromeda	730	1.733	0.999	2
LMC	68	1.628	0.999	2
SMC	45	-	-	-

straight line fit for the galactic clouds ranges from  $-1.44$  to  $-1.64$  for the various models,  $-1.51$  being the mean value. For the clouds of M31 and the LMC the slope has the values  $-1.73$  and  $-1.63$  respectively. We note here that for M31 and the Magellanic Clouds the mass estimates using only the major and minor angular dimensions are very crude and for M31 the opacity estimates are not available. With this in view it is remarkable that the mass function for clouds in M31 and the LMC is very similar to that for the galactic clouds. The dark clouds of SMC display a very small range in mass.

It is interesting that the equivalent slope for the mass function of comets has a value of  $-1.6$  (Hughes and Daniels, 1980) while for the asteroids the value is  $-1.8$  (Dohnanyi, 1969), compared to the value for the dark clouds found to be in the range  $-1.4$  to  $-1.7$ . However, the dark cloud mass functions found here are rather dissimilar to the Salpeter mass function for stars (slope  $-2.4$ ).

Turning now to the galactic cloud complexes, we note that the mass functions for the Orion and  $\rho$  Ophiuchi complexes are similar and have a slope close to  $-1$ , implying equal number of clouds in equal logarithmic mass intervals. This is very different from the mass function for the general cloud distribution in the Galaxy, in M31 and in the LMC. The Taurus complex has a mass function which is similar



to the general cloud distribution. It is possible that the Taurus complex being very close to us ( $D = 100$  pc), some background clouds have been included in the analysis which are not in reality physical members of the complex. Also it may be that the Taurus complex is really different from the Orion or the  $\rho$  Ophiuchi complexes and is closer to being part of the general distribution as the cloud complex evolves.

#### II. 5:1 The Oort Model and the Mass Distribution for Interstellar Clouds

Oort (1954) proposed a model for the formation and destruction of interstellar clouds in which small fast moving clouds are accelerated by the radiation of O and B type stars away from regions of star formation. They undergo inelastic collisions and coalesce to grow, until they reach such a mass that they are unstable to gravitational collapse. Collapse leads to star formation and the hot young stars accelerate most of the mass in the collapsing cloud back to the interstellar medium in the form of small fast moving clouds. Thus, the cycle is completed.

Oort's model has been investigated mathematically by Field and Saslaw (1965) and Penston et al. (1969) who found that the mass distribution of clouds it predicted is  $N(M) \propto M^{-1.5}$ . Penston et al. (1969) and Handbury et al.

(1977) performed computer simulations of Oort model and obtained mass functions with slopes in the range -1.5 to -1.9. It is clear that the mass distributions for dark nebulae obtained here are in very good agreement with Oort model. When a large cloud reaches the critical size in Oort model its collapse and fragmentation may give rise to cloud complexes like Orion and  $\rho$  Ophiuchi. The mass distribution of the clouds in these complexes will then be different, having formed in a different way. Our results on the Orion and  $\rho$  Ophiuchi complexes suggest that this distribution is characterized by  $N(M) \propto M^{-1}$ .

In summary, we find that the mass function for the general field of clouds is a power law  $N(M) \propto M^{-s}$ , with 's' in the neighbourhood of 1.5 in accordance with the Oort model, which the corresponding value of 's' for the cloud complexes is about 1.

## CHAPTER III

### THE DUST DISTRIBUTION IN BOK GLOBULES

#### III.1 Introduction

Over thirty years ago, Bok and Reilly (1947) pointed out the existence of small, quasi-spherical, relatively opaque interstellar clouds. These have since become known as Bok globules. They are typically a few arc minutes in angular size ( $\sim 1$  pc diameter) with average kinetic temperature  $T \sim 10$  K and extinction  $A_v \sim 5$  magnitudes. It has been suggested (e.g. Bok, 1977) that they are proto-protostars in a state of gravitational collapse and will eventually give birth to stars. For this reason it is important to know the radial density structure of these objects.

Recently two globules have been studied in some detail, B361 by Schmidt (1975) and Globule 2 in the Coalsack by Bok (1977). In both cases the authors have used star counts to measure the extinction  $A_v$  as a function of radial distance  $R$  from the globule centre. It is found that the globules have a small dark core and beyond the core the extinction varies approximately as  $A_v(R) \propto 1/R^2$ , and the derived dust density falls as  $\rho(R) \propto 1/R^3$ . This is a rather steep density gradient when compared to the gravitational collapse calculations that predict a gradient at most only as steep as  $\rho(R) \propto 1/R^2$  (Penston, 1969; Larson, 1969).

Kenyon and Starrfield (1979) have produced polytropic models for these globules and compared the extinction obtained from their calculations with that observed by Schmidt and Bok. They assume that the dust to gas ratio is normal and constant. There are, however, two effects which may raise some doubts about this picture. First, gravitational settling, where the dust grains in a globule react to the gravitational field of the globule and settle towards its centre. This phenomenon has been extensively discussed in the context of planetary formation (e.g. Williams, 1972; Williams and Handbury, 1974), but it has also recently been suggested that it may be an important mechanism in triggering star formation (Alfven and Carlqvist, 1978). The obvious effect of this phenomenon is to generate a dust concentration close to the globule centre. Second, any anisotropy in the radiation field can drive dust grains relative to the ambient gas. In general in interstellar space, the radiation is fairly isotropic and so dust grains will not be accelerated. However, in the neighbourhood of a dark cloud, the dark cloud itself generates anisotropy by obscuring radiation from a specific direction. This results in a net radiation field towards the dark cloud in the neighbouring areas which in turn drives any dust grains in the locality towards the cloud. Neighbouring OB stars can also cause considerable anisotropy in the radiation field which could drive grains towards a globule. Thus additional grains can be driven into a globule and these will subsequently also gravitationally settle. In this chapter we first discuss the

various forces which can operate on a dust grain either in the vicinity or within a dark cloud and then derive an expression for the dust density as a function of distance from the globule centre, according to the above scenario. From this the line of sight column density can be calculated which in turn is converted into extinction  $A_v$ . These theoretical results on the dust density structure and the extinction variation are compared with observations and the implications are discussed.

### III.2 Theory

Consider a dust grain of radius 'a'. If  $\Theta$  is the density of the grain material, then mass of the grain  $m = \frac{4}{3} \pi a^3 \Theta$ . We consider the grains to be spherical for simplicity. The various forces acting on the grain in the environs of a globule are the following.

#### III.2:1 Gravity:

Gravity is an obvious force that accelerates the grain towards the centre of the globule. If 'g' be the gravitational field, then the force on a grain of mass m is given by

$$F_{\text{gravity}} = mg = \frac{4}{3} \pi a^3 \Theta g \quad \text{III(1)}$$

For a spherical distribution of mass the gravitational field at a distance  $R$  from the centre is  $\frac{GM(R)}{R^2}$ , where  $M(R)$  is the mass within the radius  $R$  and  $G$  is the universal gravitational constant. Thus,

$$F_{\text{gravity}} = mg = \frac{4}{3} \pi a^3 \theta \frac{GM(R)}{R^2} \quad \text{III(2)}$$

### III. 2:2 Viscous Drag

When a dust grain experiences a force which causes it to move relative to an ambient gas, a viscous drag resists its motion. In our case, the dust grain is much smaller than the mean free path within the gas and so the drag derived by Baines, Williams and Asebiomo (1965) is valid. Baines et al. (1965) have derived an expression for drag valid for all speed ranges, but it is appropriate in our case to use an approximation that is valid when the relative speed  $v$  is less than the local mean thermal speed of the gas  $W$ , which is

$$F_{\text{drag}} = \frac{4}{3} \pi a^2 \rho_g W v, \quad \text{III(3)}$$

$\rho_g$  being the density of the resisting gas medium.

$W = \left( \frac{2kT}{M} \right)^{\frac{1}{2}}$ , where  $T$  is the gas temperature,  $M$  is the mean molecular mass and  $k$  is the Boltzmann constant.

For the situations of our interest  $T \sim 10$  K so that

$W \sim 5 \times 10^4 \text{ cm s}^{-1}$ , whereas the speed of the grains ( $a \sim 0.2 \text{ } \mu\text{m}$ ,  $\rho \sim 1 \text{ g cm}^{-3}$ ) relative to the gas, under the balance of the forces of gravity and viscosity (Equations III(2) and III(3)) turns out to be  $v \sim 10^3 \text{ cm s}^{-1}$ .

### III. 2:3 Radiation Pressure

It has long been recognised (e. g. Wickramasinghe, 1967) that if the energy density of a radiation field is  $u$  and  $\xi$  the fractional anisotropy in that field, then the force on a grain of radius  $a$  is given by

$$F_{\text{rad}} = \pi a^2 Q u \xi \quad \text{III(4)}$$

where  $Q$  is the efficiency factor, which in general is a complex function of grain radius, grain composition and frequency distribution of the radiation field.

### III. 2:4 Radiation Driven Grains and the Dust Distribution in Bok Globules

Consider a globule surrounded by interstellar matter and radiation field. The globule is a source of

obscuration and creates an anisotropy in the radiation field in its neighbourhood. Thus, outside the globule, in its immediate vicinity there is a net radiation field towards the globule. Any dust grains in this region will therefore be driven towards the globule by radiation pressure force given by Equation III(4). As the grains move relative to the ambient gas, their motion is resisted by the viscous drag force given by Equation III(3). The terminal velocity  $v$  of such radiation driven grains towards the globule is obtained by equating the two opposing forces given by Equations III(3) and III(4) and is

$$v = \frac{3 Q u \xi}{4 \rho_g W} \quad \text{III(5)}$$

Assume that outside the globule the ambient medium has the normal ratio by mass of dust to gas  $\lambda$ , then the mass flux of grains  $\dot{M}$  across the surface of the globule of radius  $R_o$  will be

$$\dot{M} = 4 \pi R_o^2 v \lambda \rho_g \quad \text{III(6)}$$

Substituting for  $v$  from Equation III(5) we get

$$\dot{M} = \left( \frac{3 \pi Q u \xi R_o^2 \lambda}{W} \right) \quad \text{III(7)}$$



When the grain meets the globule, it is decelerated by the drag of the gas in the globule since the density is much higher there. The high density and the consequent absorption in the globule also damps out the driving radiation and so the grain quickly enters a regime where the terminal velocity is determined by balancing the drag in the globule (which has the same form as Equation III(3) but with the globule density  $\rho_c$  and globule mean thermal velocity  $W_c$  inserted) against the gravitational field of the globule. The gas in the globule is assumed to be stationary and if we consider a simple model of the globule structure where for most of the globule  $\rho_c = \rho_o (R_o/R_c)^n$ , then the mass interior to the radius  $R_c$  is

$$M(R_c) = \int_0^{R_c} 4\pi R_c^2 \rho_c dR_c = \left( \frac{4\pi \rho_o R_o^n R_c^{3-n}}{3-n} \right)$$

and the gravitational field is thus

$$g = \left( \frac{4\pi G \rho_o R_o^n R_c^{1-n}}{3-n} \right) .$$

Using Equation III(2) we find the gravitational force on the grain to be

$$F_{\text{gravity}} = \left( \frac{4}{3} \pi a^3 \theta \right) \left( \frac{4 \pi G \int_0^{R_c} \rho_o R^n R_c^{1-n} dR}{3-n} \right) \quad \text{III(8)}$$

Balancing gravitational and drag forces (Equation III(8) and Equation III(3) with  $\rho_g$  and  $W$  replaced by  $\rho_c$  and  $W_c$ ) one gets for the terminal velocity of a grain within the globule

$$v_c = \frac{4 \pi G \theta a R_c}{(3-n) W_c} \quad \text{III(9)}$$

A very satisfactory feature of this expression is that it only depends in a very minor way on the density structure  $n$ . The mass flow of dust grains within the globule is

$$\dot{M} = 4 \pi R_c^2 v_c \rho_d, \quad \text{III(10)}$$

where  $\rho_d$  is dust density at a distance  $R_c$  from the globule centre. As  $\dot{M}$ , the flow rate of grains is determined by Equations III(7) and  $v_c$  by Equation III(9), Equation III(10) determines the dust density at any point within the globule as

$$\rho_d(R_c) = (\dot{M}/4\pi R_c^2 v_c) = (\lambda B R_o^2)/R_c^3, \quad \text{III(11)}$$

where  $B$  is the constant given by

$$B = 3(3-n) W_c Q u \xi \lambda / 16 \pi G \theta a W. \quad \text{III(12)}$$

The value of  $B$ , as we shall see, is important in determining the observational features of the globule. Irrespective of the value of  $B$ , the model predicts a very steep density gradient, varying inversely as the cube of the radial distance from the globule centre. This is in very good agreement with the observations of globules by Schmidt (1975) and Bok (1977) who found exactly such a radial dust density gradient ( $\rho \propto R^{-3}$ ).

The observed quantity of interest, the extinction  $A_v$  is proportional to the column density of dust, and is given by (see for example Jenkins and Savage, 1974)

$$A_v = \frac{10^3}{2} \int \left( \frac{\rho_d}{\lambda} \right) dx, \quad \text{III(13)}$$

where the integration is along a sight line through the globule. For such a sight line, passing at a distance

$R_d$  from the globule centre simple geometry gives

$$\int_d^{\rho} dx = 2 \int_0^{R_d} \frac{B \lambda R_o^2 dx}{(R_d^2 + x^2)^{3/2}}$$

$$= 2 \lambda B \left( \frac{R_o}{R_d} \right)^2 \left[ 1 - (R_d / R_o)^2 \right]^{\frac{1}{2}},$$

so that

$$A_v(R_d) = 10^3 B \left( \frac{R_o}{R_d} \right)^2 \left[ 1 - (R_d / R_o)^2 \right]^{\frac{1}{2}} \quad \text{III(14)}$$

If strictly applied, this of course implies that  $A_v \rightarrow \infty$  as  $R_d \rightarrow 0$ . This is a consequence of the density also tending to infinity at the centre, as can be seen from Equation III(11). In reality of course, at some point, the mean thermal velocity of the grains becomes important so that the pressure is then able to withstand the settling tendency of gravity and a high, but finite, density core is produced. In theory one could certainly estimate this point, but we have not done so for the following reason. When  $A_v$  approaches a value of about 10 that part of the globule becomes very opaque and there is no reliable way of observationally estimating the extinction of an opaque

body. We thus cut off the calculation at  $A_v = 10$ , rather than try to predict its value in this regime.

### III. 3 Comparison with Observations

With the exception of  $(3-n) Q u \xi$  the quantities in Equation III(12) defining  $B$  are fairly well determined. However,  $(3-n) Q u \xi$  can take a range of values depending on the environment. At the lower end, the average galactic density of radiation (Allen, 1973) is  $6 \times 10^{-13} \text{ erg cm}^{-3}$  and near a globule  $\xi \sim 1/6$  (by the usual argument that one component in one direction is blocked off).  $Q$  will be close to unity for all normal interstellar grains at the mean wavelength of the galactic radiation, while  $n$  could be close to 2. Thus a minimum value for  $B$  is  $\sim 10^{-5}$  (taking standard values for all the other parameters). At the upper end of the scale, a set of 50 OB stars produces an energy density of  $\sim 5 \times 10^{-11} \text{ erg cm}^{-3}$  within 10 pc with  $\xi \sim \frac{1}{2}$ , while the globule could be uniform with  $n = 0$ . In this event  $B$  is  $\sim 10^{-2}$ . Any value for  $B$  in the range  $10^{-5} \lesssim B \lesssim 10^{-2}$  must be considered reasonable.

By substitution into Equation III(14), it is easy to see that with  $B = 10^{-2}$ ,  $A_v \gtrsim 10$  for 80 per cent of the radius of the globule. Observationally such a globule would be described as being totally opaque all over. Similarly for

$B = 10^{-5}$ ,  $A_v \lesssim 1$  for 90 percent of the radius. Such a globule, if old enough for the dust original to the globule to have gravitationally settled, will display a dark core with relatively transparent surrounding envelope. It is interesting to note that examples of both types of globules can be found (e.g. B 68, ORI-I-2 of the first type and E 92, B 227, B 335 of the second; Bok and McCarthy, 1974; Martin and Barrett, 1978).

Our prime interest here is in the two globules referred to earlier which do not show either of these extreme characteristics, but rather show an internal smooth variation in  $A_v$ . In Figure III.1 we show the observational data by Schmidt (1975) for B 361 and also the theoretical curve given by Equation III (14) for  $E = 6.5 \times 10^{-4}$ . It should be noted that the three points near the centre were given by Schmidt, as lower bounds to the values of  $A_v$  rather than actual values, and so are not in conflict with our calculation if  $A_v \gtrsim 10$ . Similarly Figure III.2 is for Globule 2 in the Coalsack from Bok (1977). The globule is essentially opaque inside  $(R_d/R_o) = 0.3$  and no reliable estimate of extinction was possible. The value of  $B$  for the theoretical curve is  $10^{-3}$ . In both cases agreement between theory and observations is very good.

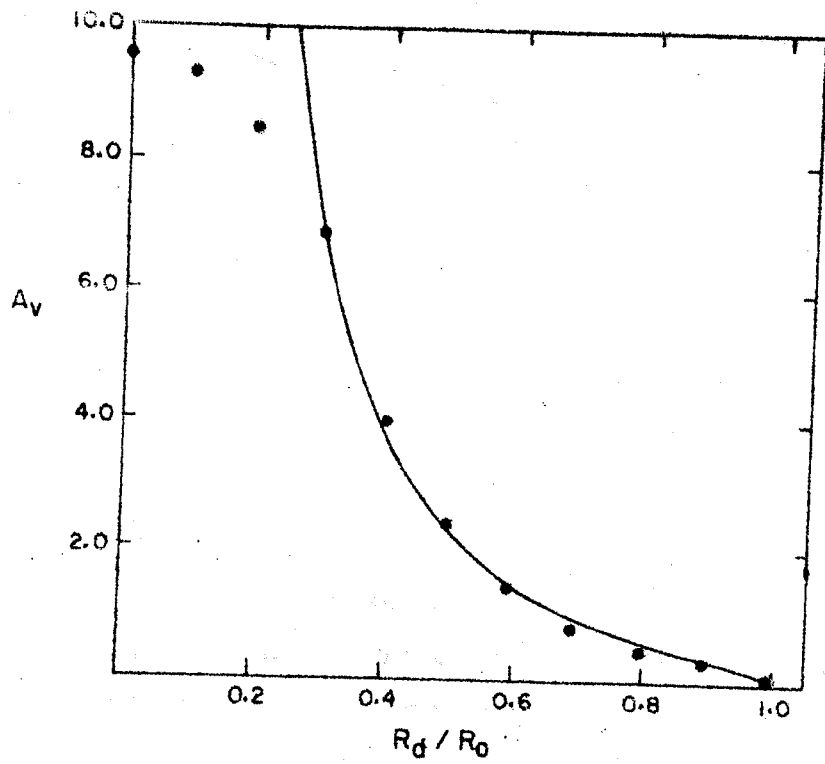


Figure III.1 : A plot of  $A_v$  against the fractional radial distance  $R_d / R_0$  from the globule centre, comparing observation (the dots) and theory (the line) for the Bok globule B 361.

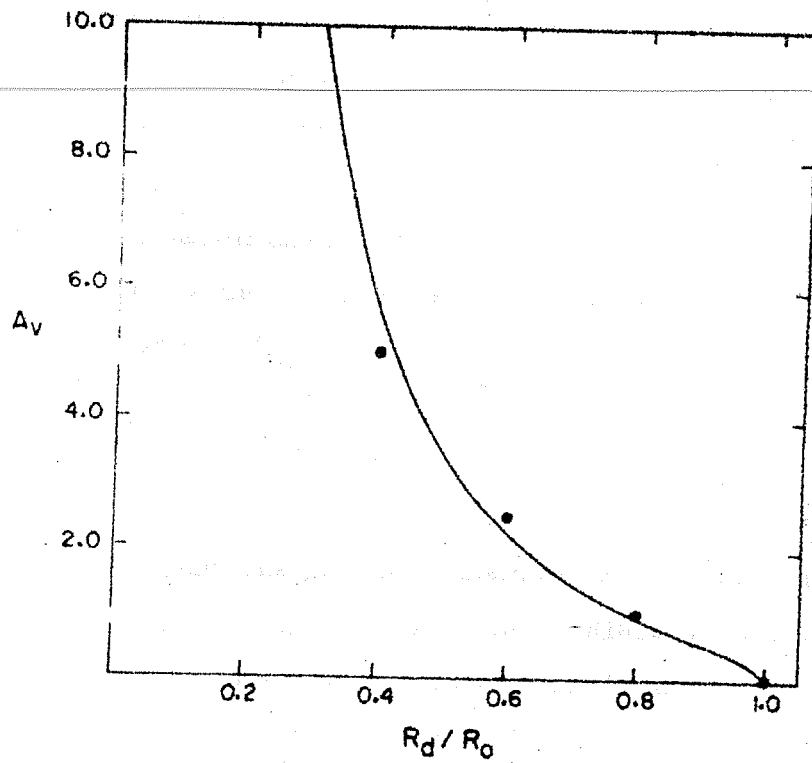


Figure III.2 : A plot of  $A_v$  against the fractional radial distance  $R_d/R_0$  from the globule centre, comparing observation (the dots) and theory (the line) for the Bok globule 2 in the Coalsack.



### III. 4 Discussion and Conclusions

We have described a scenario where dust grains settle to the centre of globules due to the gravitational field. Radiation pressure also drives in grains from the surroundings to replace these grains. If the radiation field is very strong, or the globule density very high, then a totally opaque globule ensues. If the radiation field is very weak, very little grain replacement occurs and we find globules with essentially only a dense settled core. In others, we find the situation where the replacement of grains was at a level where a density gradient across the globule is discernible, and here our predictions match the observational data.

The model that we have considered assumes that the globule is not in a state of free fall collapse. Rotation and magnetic field have been ignored, but their presence in moderate amounts would not alter the general conclusions. Grain growth, either by coagulation or condensation both of which are possibilities, will decrease the grain settling time. However, turbulence within the globule will tend to prevent settling. Dust grains being driven by radiation pressure will be present and so it seems very likely that most of the situations described above will come about in globules under different environmental conditions.

If the scenario presented in this chapter is correct, there are two important points to be made:

(1) The dust settling time  $\tau = \frac{R_c}{V}$  is easily obtainable from Equation III(9) and for typical values of the parameters, is found to be of the order of  $3 \times 10^7$  yr. Some globules must be older than this to display the observed settling characteristics and so globules must be stable on this time scale.

(2) The usually quoted globule masses are obtained from the dust content as deduced from  $A_v$ . As not all of this dust is original to the globule, the masses have been over-estimated in the past. The additional radiation driven grains will increase the dust to gas ratio in the globules. Jones et al. (1980) have published work which shows that the dust to gas ratio in Globule 2 in the Coalsack is higher than normal, thus confirming the general scenario described above.

It will be instructive to carry out detailed observations in the optical, infrared and microwave molecular lines of a representative sample of globules to determine their radial structure, average grain sizes and dust to gas ratios.

## CHAPTER IV

### SEGREGATION OF DUST GRAINS IN DARK CLOUDS

#### IV.1. Introduction

Gravitational settling of dust in cosmic gas clouds has been discussed by several authors. Dust grains under the influence of the gravitation of the cloud tend to sediment towards the center of gravity of the cloud, their motion being resisted by the gas viscosity. This phenomenon was first discussed by McCrea and Williams (1965) in the context of planetary formation. Horedt (1973, 1976) and Alfvén and Carlqvist (1978) have pointed out the importance of dust segregation in interstellar clouds for the formation of 'proto-cores' which may trigger gravitationally assisted accretion leading to star formation. As discussed in Chapter III we have shown that the settling of dust in Bok globules may be responsible for the observed radial variation of extinction in these objects. As the dust grains sediment towards the center of the globule, extinction in the inner regions of the globule increases at the expense of the extinction in the outer regions. A detailed model based on the gravitational settling of dust that is being driven into the globule by radiation pressure is found to be in good agreement with the observed radial variation of extinction within the globules B 361 and Globule 2 in

the Coalsack studied by Schmidt (1975) and Bok (1977) respectively.

In this Chapter we discuss another observable manifestation of the gravitational settling of dust grains in dark clouds. We start with a uniform spherical dust cloud. Initially, the dust is assumed to have a grain size distribution typical of the interstellar medium. Under the combined influence of the gravitational field and the viscous drag of the gas, dust grains sediment towards the center. As will be seen in Section IV.2 a dust grain of radius  $a$ , at a distance  $r$  from the center of the cloud has a settling speed  $|v| = cr$ , where  $c$  is a constant. Thus the sedimentation time scale  $\tau = |r/v| = 1/ca$ . Larger grains sediment faster. Such a size dependent settling will therefore modify the grain size distribution function of the dust. In Section IV.2 for our simple model of a uniform spherical cloud we derive an expression for the modified grain size distribution function as a function of  $r$  and time  $t$ . However, the physical quantities characterizing the dust distribution which can be directly related to the observations are: the mean grain size  $\langle a \rangle$  and the extinction  $A_\lambda$  (at wavelength  $\lambda$ ) along a line of sight through the dark cloud. One observes background stars through the intervening dust cloud. The dust in the cloud causes extinction and polarization of the light from the stars. The wavelength of maximum linear polarization  $\lambda_{\max}$  and also the ratio of total to selective extinction

$R = A_v / (A_B - A_v)$  then give a measure of the mean grain size along the line of sight. An increase in mean grain size will result in an increase in  $\lambda_{\max}$  and also  $R$  (Greenberg, 1968; McMillan, 1978). In Section IV.3 we therefore derive expressions for the mean grain radius  $\langle a \rangle$  and extinction  $A_v$  as functions of the projected radial distance  $x$  from the cloud-center and the age of the cloud  $t$ . We have numerically evaluated these quantities for various values of the age of the cloud and plotted the results in Figures IV.1 and IV.2. We find that the mean grain size as well as the extinction increases towards the center of the cloud. In Section IV.4 we discuss these results with reference to the observations of anomalous reddening and polarization within dark clouds and suggest further detailed observations of dark clouds and Bok globules.

## IV.2 Segregation of Dust and the Grain size distribution

### IV.2.1 SEGREGATION OF DUST GRAINS

Consider a spherical cloud of radius  $R_0$  and constant density  $\rho$ . Initially the dust in the cloud is uniformly mixed with the gas. The grain size distribution for the dust is typical of the interstellar medium, and is the same everywhere in the cloud. The total dust mass is only a small fraction ( $\sim 10^{-2}$ ) of the cloud mass. We therefore neglect the contribution of the dust to the gravitational field in the

cloud. Spherical symmetry is assumed. We do not take the growth of grains into consideration.

At a radial distance  $r$  from the center of the cloud the gravitational acceleration  $g$  directed towards the center will be

$$g = \frac{4}{3} \pi \rho G r \quad \text{IV(1)}$$

where  $G$  is the gravitational constant.

A spherical dust grain of radius  $a$ , density  $\theta$  and mass  $m = \frac{4}{3} \pi \theta a^3$  at the radial distance  $r$  will experience the gravitational force directed towards the center

$$F_g = mg = \left( \frac{4}{3} \pi \right)^2 G \rho \theta a^3 r \quad \text{IV(2)}$$

If the grain moves with an inward radial velocity  $v$  through the cloud, its motion will be resisted by the viscous drag force

$$F_v = \frac{4}{3} \pi a^2 \rho W v \quad \text{IV(3)}$$

where  $W$  is the mean thermal velocity of the gas molecules (Williams and Crampin, 1971).

$W = (2 kT / M)^{\frac{1}{2}}$ , where  $T$  is the temperature of the gas.  $M$  is the mean molecular mass and  $k$  is the Boltzmann constant.

Balancing the gravitational force by the viscous drag force  $F_g = -F_v$  we obtain the settling velocity

$$v = \frac{dr}{dt} = - (4 \pi G \Theta a r / 3 W) = - c a r \quad \text{IV(4)}$$

$$\text{where } c = (4 \pi G \Theta / 3 W)$$

and the settling time scale

$$\tau = \left| \frac{r}{v} \right| = (3 W / 4 \pi G \Theta a) = 1 / c a \quad \text{IV(5)}$$

It is clear from Equation IV(5) that larger grains (large  $a$ ) settle faster (small  $\tau$ ). Therefore, if we start with a distribution of grain sizes; with the passage of time the distribution will get modified. From the outer regions of the cloud larger grains will have settled towards the

inner regions, making the grain size distribution in the inner regions enhanced with larger grains. In the following we make a calculation of this effect.

#### IV.2:2 MODIFICATION OF THE GRAIN SIZE DISTRIBUTION FUNCTION

Initially (  $t = 0$  ) we assume the dust in the cloud to have the Oort-van de Hulst type grain size distribution

$$n(a) = n_0 \exp(-\sqrt{a}^3) \quad \text{IV(6)}$$

such that  $n(a) da$  is the number of grains per unit volume with radii between  $a$  and  $a + da$  (Greenberg, 1968).  $n_0$  is a normalizing factor and  $\sqrt{\phantom{x}}$  is a constant related to the characteristic grain size. Here we will use  $\sqrt{\phantom{x}} = 40 \mu\text{m}^{-3}$  (Greenberg, 1968). At  $t = 0$  the size distribution function is assumed to be the same at all points in the cloud.

From Equation IV(4) we find a relation between the position of a grain  $r(t)$  at time  $t$  and its initial position  $R_i$  as

$$r(t) = R_i \exp(-act) \quad \text{IV(7)}$$

with the constraint  $R_i \leq R_0$ .



If we consider a spherical shell of radius  $r$  and thickness  $dr$ , then at time  $t$ , all the grains with radii between  $a$  and  $a+da$  in this shell must have settled down from another shell with radius  $R_i$  and thickness  $dR_i$ ,  $r(t)$  and  $R_i$  being related by Equation IV(7). If the new grain size distribution function at position  $r$  and at time  $t$  be  $n(a, r, t)$ ; by conservation of dust grains we obtain

$$4\pi r^2 dr n(a, r, t) da = 4\pi R_i^2 dR_i n(a, R_i, 0) da \quad \text{IV(8)}$$

using  $n(a, R_i, 0) = n_0 \exp(-\sqrt[3]{a})$  for the initial distribution function, and Equation IV(7) relating  $r$  and  $R_i$  we get

$$\begin{aligned} n(a, r, t) &= n(a, R_i, 0) \exp(3act) \\ &= n_0 \exp(3act - \sqrt[3]{a}) \end{aligned} \quad \text{IV(9)}$$

The constraint  $R_i \leq R_0$  in Equation IV(7) can also be written as

$$a \leq a_{rt} = (1/ct) \ln(R_0/r)$$

Grains with  $a > a_{rt}$  will have all crossed the spherical

surface with radius  $r$  as they settle towards the center of the cloud. Therefore at time  $t$  we get for the modified grain size distribution function

$$n(a, r, t) = \begin{cases} n_0 \exp(3act - \gamma a^3) & \text{for } a \leq \left(\frac{1}{ct}\right) \ln(R_o/r) \\ 0 & \text{for } a > \left(\frac{1}{ct}\right) \ln(R_o/r) \end{cases}$$

IV(10)

We thus see that the grain size distribution function is now a function of time as well as of the position in the cloud. The factor  $\exp(3act)$  tends to shift the distribution towards larger grains, and there is a cut-off at  $a = a_{rt} = \left(\frac{1}{ct}\right) \ln(R_o/r)$ . Making use of the modified size distribution function derived above we can now calculate the average grain size and extinction along a line of sight through the dark cloud. These quantities are directly related to the observations of extinction and polarization produced by the cloud.

### IV.3 MEAN GRAIN SIZE AND EXTINCTION

#### IV.3:1 THE MEAN GRAIN SIZE

The average grain radius  $\langle a(r, t) \rangle$  at a radial

distance  $r$  in the cloud at time  $t$  can be written as

$$a(r, t) = \frac{\int_0^{a_{rt}} a n(a, r, t) da}{\int_0^{a_{rt}} n(a, r, t) da} = \frac{\int_0^{a_{rt}} a \exp(3 act - \sqrt[3]{a^3}) da}{\int_0^{a_{rt}} \exp(3 act - \sqrt[3]{a^3}) da}$$

IV(11)

$$\text{where } a_{rt} = (1/ct) \ln(R_o/r)$$

However, the average quantity of greater observational interest is the average grain radius  $\langle a(x, t) \rangle$  along a line of sight through the cloud passing at a projected radial distance  $x$  from the center of the cloud. For the geometry under consideration, performing the integrations along the line of sight, the average grain radius  $\langle a(x, t) \rangle$  is found to be given by

$$a(x, t) = \frac{\int_0^{a_{xt}} a \left\{ \exp(-2 act) - (x/R_o)^2 \right\}^{\frac{1}{2}} \exp(3 act - \sqrt[3]{a^3}) da}{\int_0^{a_{xt}} \left\{ \exp(-2 act) - x/R_o^2 \right\}^{\frac{1}{2}} \exp(3 act - \sqrt[3]{a^3}) da}$$

IV(12)

$$\text{where } a_{xt} = (1/ct) \ln(R_o/x)$$

#### IV.3:2 EXTINCTION

The extinction  $A_\lambda$  at wavelength  $\lambda$ , along the line of sight can be written as

$$A_\lambda = \int N(a) C_{\text{ext}}(a, \lambda) da \quad \text{IV(13)}$$

where  $N(a)$  is the column density of grains with radii between  $a$  and  $a+da$ , along the line of sight and  $C_{\text{ext}}$  is the extinction cross-section of grains. For  $C_{\text{ext}}$  we use the following approximation (Greenberg, 1978).

$$C_{\text{ext}} = \pi a^2 \left\{ 2 - 4 \xi^{-1} \sin \xi + 4 \xi^{-2} (1 - \cos \xi) \right\} \quad \text{IV(14)}$$

$$\text{where } \xi = 4 \pi (a/\lambda) (m' - 1)$$

and  $m' =$  index of refraction of the grains.

With this approximation for the extinction cross-section and performing the line of sight integration we get for extinction

$$A_{\lambda}(x, t) = 2\pi n_0 R_0 \int_0^{a_{xt}} a^2 \left\{ \exp(-2act) - (x/R_0)^2 \right\}^{\frac{1}{2}} * \\ * \exp(3act - \sqrt{a^3}) \left\{ 2 - 4\zeta^{-1} \sin\zeta + 4\zeta^{-2} (1 - \cos\zeta) \right\} da$$

IV(15)

$$\text{where } a_{xt} = (1/ct) \ln(R_0/x)$$

Equations IV(12) and IV(15) thus give the expressions for the mean grain radius  $\langle a(x, t) \rangle$  and extinction  $A_{\lambda}(x, t)$  respectively, along a line of sight through the cloud as functions of the projected radial distance  $x$  from the center of the cloud and the age  $t$  of the cloud.

#### IV. 3:3 NUMERICAN RESULTS

Using Equations IV(12) and IV(15) we have numerically evaluated the quantities  $\langle a(x, t) \rangle$  and  $A_v(x, t)$  (extinction in the visual,  $\lambda \simeq 0.55 \mu\text{m}$ ) for various values of the cloud-age  $t$ , and studied their variation with radial distance  $x$  across the cloud. The values used for the different parameters appearing in the expressions for  $\langle a(x, t) \rangle$  and  $A_v(x, t)$ , and characterizing the dust

cloud are :  $\gamma = 40 \mu m^{-3}$ ,  $\Theta = 1 \text{ gm cm}^{-3}$ ,  $m' = 1.33$ ,  $T = 10 \text{ K}$ ,  $R_o \simeq 1 \text{ pc}$  and  $n_o \simeq 10^{-13} \text{ cm}^{-3}$ . These values are typical of the interstellar dust and dark clouds (Greenberg, 1968; Martin and Barrett, 1978).  $\gamma = 40 \mu m^{-3}$  yields the mean grain radius for the normal interstellar dust  $\langle a \rangle \simeq 0.15 \mu m$ .  $R_o = 1 \text{ pc}$  and  $n_o = 10^{-13} \text{ cm}^{-3}$  would correspond to a typical Bok globule with number density of hydrogen molecules  $n_{H_2} \sim 10^4 \text{ cm}^{-3}$ , gas to dust ratio  $\sim 10^2$  and average grain radius  $\sim 0.15 \mu m$ . It turns out that the constant  $c \simeq 10^{-11} \text{ cm}^{-1} \text{ sec}^{-1}$ .

We have performed the calculations for  $t = 1, 2, 4, 8, 16, 32, 64$  and  $128$  million years. In Figure IV.1 we plot the average grain radius  $\langle a \rangle$  against the fractional radial distance  $x/R_o$  for various illustrative values of  $t$  (curves corresponding to the different values of  $t$  have been marked with numbers representing the cloud age  $t$  in units of one million years). Similarly in Figure IV.2  $A_v$  has been plotted against  $x/R_o$ . Here the product  $n_o R_o$  appearing in Equation IV(15) for extinction has been so chosen that  $A_v(o, o) = 5$  magnitudes. There is no loss of generality in choosing  $n_o R_o$  arbitrarily.

#### IV. 4 Discussion and Conclusions

From Figure IV.1 we find the following:

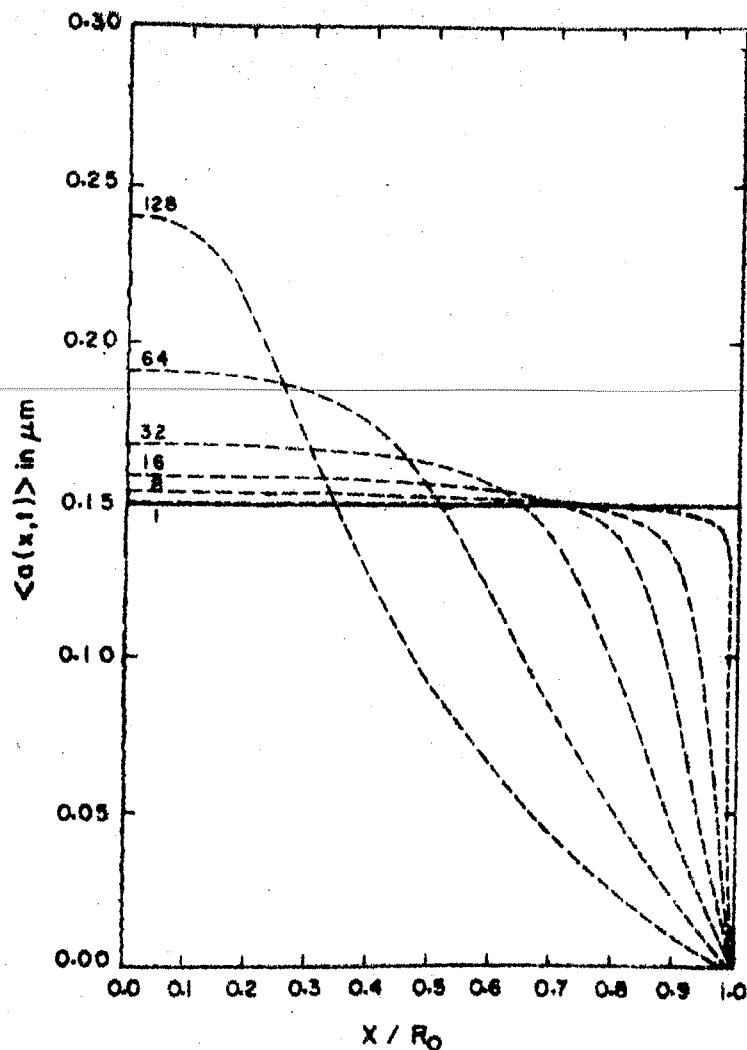


Figure IV.1 : Plot of the average grain radius  $\langle a \rangle$  against the fractional radial distance  $X/R_0$  for various values of  $t$ . The curves for different values of  $t$  have been marked with numbers representing the values of  $t$  in million yr. The solid line corresponds to the cloud at  $t = 0$  when  $\langle a \rangle$  has the same value at all points in the cloud and is equal to the value for the normal interstellar medium ( $\langle a \rangle = 0.15 \mu m$ ).

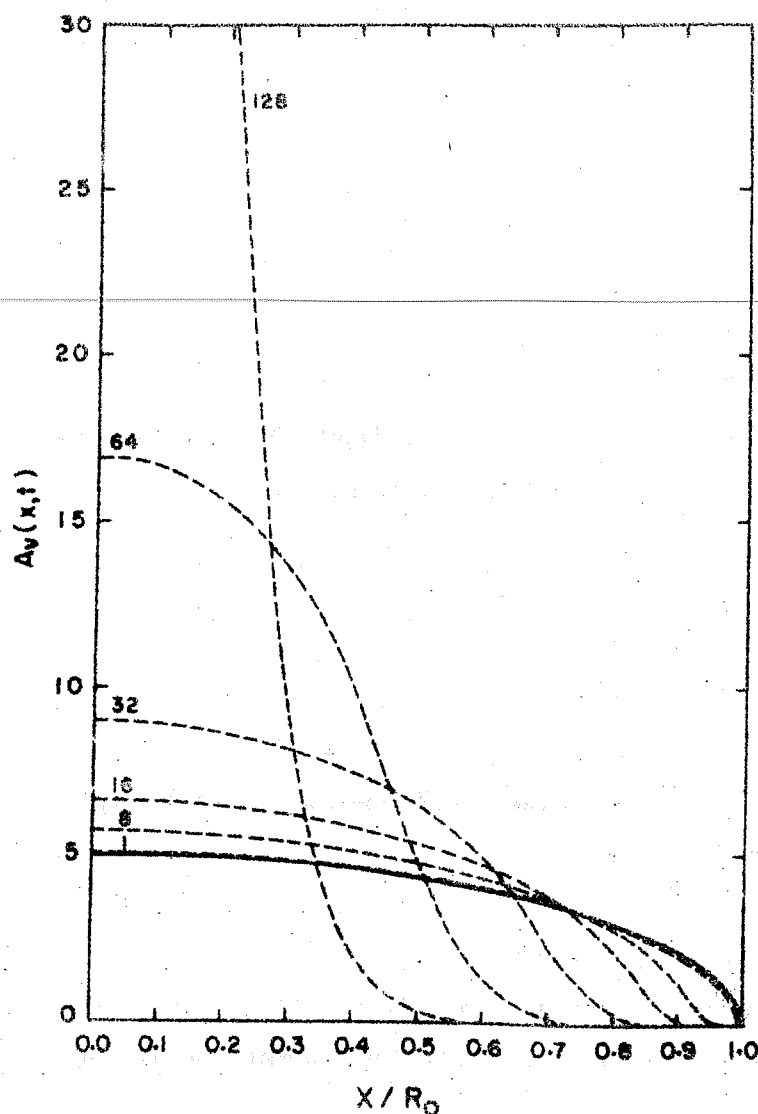


Figure IV.2 : Plot of extinction  $A_v$  against the fractional radial distance  $X/R_0$ . The curves for different values of  $t$  have been marked with numbers representing values of  $t$  in million yr. The solid curve is for  $t = 0$ . For  $t = 128$  million yr.  $A_v$  approaches the value  $\approx 65$  as  $X/R_0 \rightarrow 0$ .



1. At any given time  $t > 0$ , the mean grain radius  $\langle a \rangle$  decreases monotonically with increasing radial distance  $x/R_0$ .
2. For small values of  $t$  ( $t < 10^7$  yr.) the mean grain radius over most of the cloud (i.e. for  $x/R_0 \lesssim 0.8$ ) is the same and is close to the interstellar value  $\langle a \rangle \simeq 0.15 \mu\text{m}$ . Only in the outer most regions ( $x/R_0 \gtrsim 0.8$ ) the mean grain radius begins to be appreciably smaller than the interstellar value.
3. With increasing age ( $t > 10^7$  yr.) the mean grain radius in the inner regions of the cloud ( $x/R_0 \lesssim 0.5$ ) increases to values appreciably larger than the interstellar value.
4. The average grain radius in the inner regions of the cloud increases at the expense of the outer regions where this average decreases below the interstellar value. The point which separates these two regions shifts to smaller  $x/R_0$  values with increasing cloud age  $t$ .

At this stage we would like to point out a limitation of the present calculation. The lower limit of integration in Equations IV(12) and IV(15) have been taken to be zero. Thus, it has been assumed that the process of gravitational

settling occurs for even the smallest of the grains with  $a \rightarrow 0$ . However, grains smaller than some small radius  $a_1$  will not settle. This happens when the thermal velocity of the grains becomes greater than their settling velocity. For the parameters of the typical cloud under consideration  $a_1 \sim 0.01 \mu\text{m}$ . Therefore even in the outermost regions of the cloud, the mean grain radius will not fall below the value  $\sim 0.01 \mu\text{m}$ . Inclusion of the size range 0 to  $a_1$  in the integrals in Equations IV(12) and IV(15) does not affect the results because the contribution to the integrals is very small. In any case the qualitative results of our calculations will hold. Any other different set of parameters of the dust cloud also gives the same qualitative behaviour for the dust in the cloud as presented in Figures IV.1 and IV.2.

Figure IV.2 shows that the radial gradient in extinction  $A_V$  becomes steeper with increasing  $t$ . Gravitational settling tends to make the inner regions of the cloud darker (high  $A_V$ ). Very old clouds ( $t \sim 10^8$  yr.) have large extinction within  $x/R_0 \sim 0.3$ , and beyond  $x/R_0 \sim 0.3$  extinction decreases to very small values. In such clouds dust has settled to form dark cores, surrounded by more transparent outer regions. Some Bok globules (B 92, B 227, B 335 for example) studied by Bok and McCarthy (1974) could be examples of clouds where this could have happened.

The variation of the grain size distribution function (and hence the mean grain size) across the cloud has very interesting implications for the observations of anomalous reddening and polarization within dark clouds. Dust in a dark cloud causes extinction and polarization of the light from background stars (For simplicity in the calculations we had taken the grains to be spherical, but in reality they would be nonspherical and thus be able to produce polarization. However, our conclusions about the grain size distribution would remain valid). The wavelength dependence of extinction and linear polarization is determined by the grain size distribution. In particular, the ratio of total to selective extinction  $R (= A_V / (A_B - A_V))$  and the wavelength of maximum linear polarization  $\lambda_{\max}$  are related to the mean grain size  $\langle a \rangle$  along the line of sight (Greenberg, 1968; McMillan, 1978).  $\lambda_{\max}$  is proportional to the average grain radius  $\langle a \rangle$  (e.g. McMillan, 1978) and Serkowski et al. (1975) find a correlation between  $\lambda_{\max}$  and  $R$  as  $R \simeq 5.5 \lambda_{\max} (\mu m)$ . For the normal interstellar medium  $\lambda_{\max} \simeq 0.545 \mu m$  and  $R \simeq 3$ .

It is clear from the above discussion that in dark clouds where the process of gravitational settling of dust has been at work, we may expect the following:

1. Existence of anomalous reddening because the grain size distribution has been altered.
2. Values of  $R$  and  $\lambda_{\max}$  higher than the interstellar values, in the inner regions of the cloud, and smaller in the outer regions.
3. Radial variation of  $R$  and  $\lambda_{\max}$  similar to the variation of the average grain radius  $\langle a \rangle$  (because  $R$  and  $\lambda_{\max}$  both are roughly proportional to  $\langle a \rangle$ ) as shown in Figure IV.1.
4.  $R$  and  $\lambda_{\max}$  would have a correlation with extinction  $A_v$  in the cloud in the sense that  $R$  and  $\lambda_{\max}$  both increase with  $A_v$  as the radial distance from the center decreases.

It should be noted here that it would be difficult to define the outer boundary of a dark cloud by means of extinction measurements. The outermost regions where we expect the mean grain size to be smaller than the interstellar value would also have very small extinction and amount of polarization. For these regions the interstellar medium may have significant contribution to the total amount of extinction and polarization along the line of sight. To our knowledge, detailed studies of the radial

variation of  $R$  and  $\lambda_{\max}$  in dark clouds have not been made. However, we note that Carrasco et al. (1973) found evidence for an increase in average grain radius, above the interstellar value in  $\rho$  Oph dark cloud and Turnshek et al. (1980) found a similar increase in average grain radius in NCC 1333. A correlation between  $\lambda_{\max}$  and extinction was also found. The increase in grain size has been customarily interpreted as grain growth by condensation of heavy elements or coagulation of grains in dense clouds. Though the conditions favourable for grain growth certainly exist in dark clouds, the gravitational settling of dust grains discussed in this Chapter offers another mechanism that can give rise to an increase in the average **grain size in the central** regions of dark clouds, especially for the old ones ( $t > 10^7$  yr.).

We suggest that detailed studies of the wavelength dependence of extinction and linear polarization within dark clouds and Bok globules be undertaken. Variation of  $R$  and  $\lambda_{\max}$  with radial distance may help us test the idea that the anomalous reddening and polarization in these objects is caused by dust that is gravitationally settling towards the center. However, the processes of grain growth and gravitational settling may both be at work in any given dark cloud.

## CHAPTER V

### POLARIMETRIC OBSERVATIONS OF THE BOK GLOBULE B 361

#### V.1 Introduction

Bok globule B 361 is a galactic dark cloud in the constellation Cygnus. It is circularly symmetric on the sky and has an angular radius of about  $12'$  centered at ( $\alpha_{1950} = 21^{\text{h}} 10^{\text{m}} 39^{\text{s}}.9$ ,  $\delta_{1950} = 47^{\circ} 10' 28''$ ). Schmidt (1975) studied B 361 by the methods of star counts and photometry. He estimated that the globule is at a distance of  $350 \pm 50$  pc and has a mass of about  $80 M_{\odot}$ . The dust density distribution in the globule is very steep, varying in the outer parts of the globule roughly as the inverse cube of the radial distance from the centre. Milman (1977) observed B 361 in the spectral lines of CO whereas Clark and Johnson (1982) used the OH and  $\text{H}_2\text{CO}$  molecular lines. They found that the gas density also increased towards the centre and the kinetic temperature of the gas is 8.5 K. The observed systematic Doppler shift of the spectral lines across the globule suggests that the globule is rotating roughly about an axis in the NE-SW direction. Fischer et al (1979) and Keene (1981) have observed B 361 in the near and far infrared. These studies indicate that the globule is heated by the interstellar radiation field and cools by emission in the far infrared and molecular lines.

Two theoretical models for this globule have been proposed. One is a polytropic model for the gas by Kenyon and Starrfield (1979) and the other one by us (Williams and Bhatt, 1982) based on the settling of dust grains as discussed in Chapter III. Schmidt (1975) as well as Kenyon and Starrfield (1979) concluded that the globule should be collapsing gravitationally for the observed gas temperature of 8.5 K, while Clark and Johnson (1982) have suggested that the globule might be in a stable configuration with rotation and magnetic polar support against gravity. However, nothing is known observationally about the strength and geometry of any magnetic field in this globule. As will be discussed in section V.2 polarization measurements can yield information regarding the magnetic field and so we have carried out polarimetric observations of the globule under consideration. In this chapter we present the results of our polarimetric observations of stars in the region of the globule B 361 and discuss the implications. These observations are the first polarimetric measurements ever made on any Bok globule.

## V.2 Aims of the Polarimetric Observations:

If the dust grains in the globule are non-spherical and aligned, star light passing through the globule will undergo polarization. Assuming that the Davis-Greenstein

(Davis and Greenstein, 1951) mechanism is responsible for grain alignment, the direction of polarization vectors (the  $E$  vectors) will be the same as the projected magnetic field direction in the globule. The amount of polarization depends on the amount of dust and the alignment efficiency which in turn is related to the strength of the magnetic field. The wavelength dependence of linear polarization depends on the distribution of the dust grain sizes. It has been shown that the wavelength  $\lambda_{\text{max}}$  at which the linear polarization attains its maximum value is proportional to the mean grain size (e.g., McMillan, 1978). We made measurements of linear polarization on stars in the area of B 361 with the following aims:

- (i) to obtain the amount and direction of polarization caused by the globule, which give information regarding the strength and geometry of the magnetic field in the globule.
- (ii) to study the wavelength dependence of polarization in order to estimate the mean grain size of dust in the globule relative to the interstellar medium. This would test the idea discussed in Chapter IV, that the grain size distribution in globules would get modified as the larger grains settle towards the



globule centre and thus reduce the mean grain size in the outer parts of the globule.

We thus expect  $\lambda_{\max}$  in the outer regions of the globule to be less than the normal value and in the inner regions of the globule it would be higher than normal.

The normal value of  $\lambda_{\max}$  for the interstellar medium is  $\simeq 0.55 \mu\text{m}$ .

### V.3 The Observations

The observations were carried out in September 1982 using the 60" I.R.F.C. at Tenerife with the Royal Greenwich Observatory polarimeter. Polarization measurements were obtained for eight of the stars studied photometrically by Schmidt (1975). One star which was not investigated by Schmidt has been observed by us and we have labelled it as 'u'. In addition to these nine stars, we also observed two stars (stars 5 and LX, using Schmidt's notation) which were considered by Schmidt to be foreground stars. We will use Schmidt's numbering system for stars throughout in this chapter.

Measurements were made using each of the filters U, B, V, R and I. In order to correct for sky polarization, observations were taken, both before and after

each measurement on a star, of the sky in the neighbourhood of the star and the corresponding Stokes parameters subtracted. The instrumental polarization was evaluated by observing the bright star SAO 50526. This gave a polarization level of 0.02% so that the instrumental polarization is negligible.

#### V.4 Results

##### V.4:1 Polarization:

The stars observed for linear polarization are listed in Table V.1. The polarization measurements were made in each of the five filters U, B, V, R, I. However, except when studying wavelength dependence of polarization for star 12, to improve the accuracy in the derived quantities (percentage polarization  $P$  and the position angle of polarization  $\Theta$ ) we have combined the results from all the filters. The results are presented in Table V.1. The polarization  $P$  and the standard deviation of  $P$ ,  $\sigma_p$  are given as percentage values. The position angle of the polarization vector  $\Theta$  and the corresponding standard deviation  $\sigma_\Theta$  are given in degrees. It should be noted that  $\sigma_p$  and  $\sigma_\Theta$  arise primarily from photon noise.  $\Theta$  is measured from North increasing Eastward and all angles are recorded in the range  $0^\circ < \Theta < 180^\circ$ . Data for stars in Table V.1 regarding their identification, V magnitude, spectral class,

Table V.1

Bok Globule B 361 : Polarimetry Results

STELLAR DATA					POLARIZATION RESULTS				
Star	V (m)	Spect- ral Class	Dist- ance (pc)	E <sub>b-y</sub> (m)	Angular Distance r ( ' )	Polari- zation P(%)	Standard Deviation $\sigma_p$ (%)	Position Angle $\Theta$ (o)	Standard Deviation $\sigma_\Theta$ (o)
5	12.31	F7 V	140	0.069	1.6	0.61	0.48	12	23
6	11.73	F4 V	300	0.218	3.6	1.04	0.37	174	10
8	13.67	B4 IV	2960	0.773	7.7	2.88	1.09	95	11
9	12.22	A4 V	570	0.492	11.4	0.57	0.39	68	20
10	12.45	F6 V	420	0.150	7.7	0.74	0.38	11	15
11	11.46	A0 V	650	0.233	5.8	1.92	0.36	12	5
12	9.61	B9 V	410	0.109	10.9	0.78	0.10	1	4
16	11.14	-	-	-	4.9	0.13	0.18	-	-
L	12.4*	-	-	-	2.9*	1.39	0.68	179	14
LX	13.3*	-	-	-	0.5*	0.29	1.09	-	-
u	12.4*	-	-	-	6.0*	1.48	0.42	74	8

\* Determined by us.

distance from us  $D$ , colour excess  $E_{b-y}$  and the angular distance from the globule center  $r$  in arc minutes have been taken from Schmidt (1975) when possible. For stars that show low polarization such that  $\sigma_p > P$ , any meaningful position angle  $\Theta$  can not be found.

#### V. 4:2 Discussion of Results on Polarization:

In order to obtain information regarding the dust and magnetic field in the globule from the polarization observations only those stars should be considered for which the observed polarization is mainly caused by the globule. For this reason we should identify and exclude the foreground stars, the light from which never passed through the globule. Similarly the very distant stars should also be excluded because their light is polarized to a large extent by the intervening interstellar medium.

We note from Table V.1 that star 8 is at 3 k pc and displays a polarization value of 2.88% which is the largest of all in the table. Also the position angle for star 8 is nearly orthogonal to that for most of the nearby stars. We conclude that star 8 is in essence showing interstellar polarization and gives no information about the globule. Star 'u' also shows a position angle for polarization that is nearly orthogonal to the general trend. No information regarding the spectral class and distance to this star is

available . From our multicolour photometry accompanying polarimetry we found for star 'u' :  $V = 12.4$  and  $(B-V) = 1.40$ . Star 'u' therefore could be an early B type star at about 1.5 kpc suffering about 4 magnitude extinction. Part of this extinction is caused by the globule and the rest by the interstellar medium. We thus consider stars 8 and 'u' as distant stars reddened and polarized to a large extent by the interstellar medium.

Stars 5 and LX were considered to be foreground stars by Schmidt (1975). They are within 3' of the globule centre. If these stars were background to the globule, light from them would suffer an extinction greater than about 7 magnitudes and one would expect a large polarization too. The observed polarization is small and we confirm the suggestion made by Schmidt that these stars are foreground to the globule. Star 16 is a late type star (Schmidt, 1975) and our photometry for it gives :  $V = 11.2$  and  $(B-V) = 0.85$ . It could be a late G type star at about 150 pc suffering very little extinction. It also shows a very low value of polarization. We conclude that star 16 is a foreground star.

Star 9 is peculiar. It was suspected by Schmidt to be a variable. It is right on the edge of the globule in projection on the sky, has a large colour excess but a low value of polarization. This star could well have circumstellar matter that produces little polarization but a large colour excess  $E_{b-y}$ .

Star L is interesting. It was suggested by Schmidt to be a foreground star. We find a polarization of 1.39% which has a position angle similar to that for the rest of the nearby background stars. But it could not be a background star because it is within 3' of the globule centre in which case it would undergo a very large extinction and polarization. Photometry for this star gives :  $V = 12.4$  and  $(B-V) = 1.09$ . It could either be a foreground K type star with a large polarization that is then difficult to understand or the star could be an A type embedded in the front of the globule so that in the latter case its light is reddened and polarized by the dust in the outer parts of the globule. The situation for stars 6, 10, 11 and 12 is clear. They are all nearby background stars and their observed polarization is mainly caused by the globule.

In Fig. V.1 we show a map indicating the polarization vectors (lengths proportional to the degree of polarization) for those stars for which the observed polarization can be attributed to the globule, namely stars 6, 10, 11, 12 and L. It is evident that the polarization vectors are all roughly parallel and point in the N-S direction. Assuming that the grains in the globule are aligned by the Davis-Greenstein mechanism this requires a magnetic field in the same direction.

B 361 is a dense globule with the number density of



hydrogen atoms  $n_H \sim 10^4 \text{ cm}^{-3}$  in the core (Milman, 1977) and  $\sim 10^3 \text{ cm}^{-3}$  averaged over the globule. The grain-gas collisions will therefore be more frequent when compared with the situation for the normal interstellar medium. Since collisions tend to destroy grain alignment, we need a higher magnetic field in the globule to attain grain alignment and produce the observed degree of polarization. Following Greenberg (1978) we estimate the required magnetic field  $B$  as

$$B^2 = 0.5 a n_H T_d T_g^{\frac{1}{2}},$$

where  $B$  is in  $\mu$  gauss,  $a$  is the average grain size in  $\mu\text{m}$ ,  $T_d$  is the dust temperature and  $T_g$  is the gas temperature. Using the typical values :  $a = 0.15 \mu\text{m}$ ,  $n_H = 10^3 \text{ cm}^{-3}$ ,  $T_d \simeq T_g = 10 \text{ K}$ , we obtain  $B \simeq 50 \mu$  gauss. Thus the globule might be threaded with magnetic field lines parallel to the N-S axis with a strength of about  $50 \mu$  gauss. We note here that the direction of the field is in the NE-SW direction. It is interesting that Clark and Johnson (1982) also deduce that a field of this strength with a direction not parallel to the rotation axis must be present in B 361 in order to account for its apparently spherical shape despite a fast rotation.



### V. 4:3 Wavelength Dependence of Polarization:

The relation between  $\lambda_{\max}$ , the wavelength at which the linear polarization attains its maximum value  $P_{\max}$  and the polarization  $P_{\lambda}$  at another wavelength  $\lambda$  has been known to follow (e.g. Serkowski, 1968; Coyne et al., 1974).

$$\ln (P_{\max}/P_{\lambda}) = 1.15 \ln^2 (\lambda_{\max}/\lambda) .$$

Using this relation we can obtain a value for  $\lambda_{\max}$  from any set of two or more observations at different wavelengths. Only for star 12 the polarization observations at B ( $\lambda = 0.44 \mu\text{m}$ ), V ( $0.55 \mu\text{m}$ ) and R ( $0.70 \mu\text{m}$ ) are sufficiently accurate so that a reliable  $\lambda_{\max}$  could be calculated. The observed values for star 12 were :

$\lambda$	P (%)	$\sigma_p$ (%)
B	0.84	0.18
V	0.83	0.17
R	0.72	0.16

From these, using the relation mentioned above we obtain

$\lambda_{\max} = 0.48 \mu\text{m}$  with  $\sigma_{\lambda} = 0.05 \mu\text{m}$ . The normal interstellar medium is characterised by  $\lambda_{\max} = 0.55 \mu\text{m}$ .

We thus believe that star 12 could be showing the polarization peaking at a wavelength below the normal value. Since

$\lambda_{\max}$  is proportional to the average dust grain size (e.g., McMillan, 1978) it appears that the dust grains causing the polarization for star 12 are of an average size smaller than the normal interstellar value. Now star 12 is projected near the outer edge of the globule B 361 and hence it may be concluded that the mean dust grain size in the outer regions of the globule is smaller than normal. This is consistent with the prediction based on the grain segregation process discussed in Chapter IV that the larger grains could have gravitationally settled to the centre, thus leaving the mean grain size in the outer parts of the globule smaller. Unfortunately it has not been possible to evaluate  $\lambda_{\max}$  with precision for any star showing through the inner parts of the globule.

## V. Conclusions

We have measured the degree of polarization and the position angle of polarization for stars in the region of Bok globule B 361. For stars whose observed polarization could be attributed to the globule we found that the polarization vectors are all roughly parallel to the

N-S axis. The globule therefore has an embedded magnetic field in the N-S direction and is inclined to the rotation axis by about  $45^{\circ}$ . The inferred strength of the magnetic field is about 50  $\mu$  gauss and is consistent with the suggestion of Clark and Johnson (1982) that the globule is in equilibrium with rotation and polar magnetic support (arising from a magnetic field that is not aligned with the rotation axis) against gravity. The mean grain size in the outer regions of the globule may be smaller than the normal interstellar value consistent with the process of gravitational settling of larger grains in the globule as described in Chapter IV. More extensive observations of B 361 and other globules are desirable.

## CHAPTER VI

### THE PULSE-PERIOD DISTRIBUTION OF BINARY X-RAY PULSARS

#### VI.1 Introduction

There are at least seventeen X-ray pulsars known to exist, with X-ray luminosities in the range  $10^{33} \lesssim (L_x/\text{erg sec}^{-1}) \lesssim 10^{39}$ , and pulse periods in the range  $1 \lesssim P (\text{sec}) \lesssim 1000$  (see Table VI.1). The most widely accepted model for these X-ray pulsars involves a rotating magnetised compact object accreting matter from a normal companion star in a binary system (Rappaport and Joss, 1977 a). The normal star supplies matter to the compact object by either a stellar wind or Roche-lobe overflow. The gravitational potential energy of the matter accreting onto the compact object powers the X-ray luminosity, and the rotation period of the compact object is identified as the X-ray pulse period. The compact objects in these binary X-ray pulsars seem to be neutron stars (Rappaport and Joss, 1977 b). We adopt this binary model for the X-ray pulsars and thus do not consider the Crab Nebula pulsar (which is not a binary system) and the X-ray pulsations observed in some cataclysmic variables like SS Cygni (Cordova et al. 1980) where the compact object is a white dwarf and the rotational origin of the pulsation is not certain.

In the pulse period distribution of the binary X-ray pulsars, several workers (e.g., Rappaport and Joss, 1977 a) have noted the apparent existence of a gap ranging from  $P \sim 10$  s to  $P \sim 100$  s. However, recently two X-ray pulsars have been discovered (White and Pravdo, 1979 ; Kelley et al., 1980) with periods that fall in this gap. Our aim in this chapter is, to show that the gap in the pulse-period distribution is significant, and to provide an explanation for this gap in terms of the character of mass transfer in the binary system.

## VI.2 The Pulse-period Distribution

In Table VI.1, we list the seventeen confirmed X-ray pulsars. The pulse-period  $P$  and where known, the spin-up time scale  $T_s = -P/\dot{P}$  ( $\dot{P}$  is the average time derivative of  $P$ ), the average X-ray luminosity  $L_x$  and the type of the optical companion are also listed. Three probable X-ray pulsars A 1239-59 (191 s), 4U 1813-14 (1913 s) and 4U 1700-37 (97 min) have not been listed, their cases being less certain (Bradt et al., 1979).

From an inspection of Table VI.1, we note the following :

1. There are five X-ray pulsars in the period range 0.7 s to 10 s, ten in the range

Table VI.1

Observed properties of binary X-ray pulsars:

Source *	Pulse-period P(s) *	Average spin-up time scale $T_s$ (years) +	Average X-ray Lumi- nosity $L_x (10^{37} \text{ erg sec}^{-1})$	Type of the optical companion *
4U 0115-73 = SMCX-1	0.71	$1.3 \times 10^3$	50	Early type
4U 1653+35 = Her X-1	1.24	$3.3 \times 10^5$	1	Low mass
4U 0115 + 63	3.61	$3.1 \times 10^4$	$\geq 0.9$	Early type
4U1118-60 = Cen X-3	4.84	$3.6 \times 10^3$	5	Early type
4U 1627-67	7.68	$5.4 \times 10^3$ <sup>a</sup>	$2(D/10 \text{ kpc})^2$ <sup>b</sup>	Low mass
2S 1417-62 <sup>c</sup>	17.64 <sup>c</sup>	50 ? <sup>c</sup>	$1(D/10 \text{ kpc})^2$ <sup>c</sup>	---
OA O 1653-40 <sup>d</sup>	38.22 <sup>d</sup>	--	$1.2(D/10 \text{ kpc})^2$ <sup>d</sup>	Early type ? <sup>e</sup>
A0535 + 26	104	29	6	Early type
4U1728-24=GX 1+4	116	50	4	Late type giant
4U1258-61=GX 304-1	272	--	$7 \times 10^{-3}$ <sup>f</sup>	Early type
4U0900-40=Vela X-1	283	$1.0 \times 10^4$	0.1	Early type

.....2/.

Table VI.1 contd.

---

4U1145-61 <sup>g, h</sup>	291 <sup>h</sup>	$> 1.0 \times 10^4$ h	$2 \times 10^{-3}$ g, h	Early type
1E1145.1-6141 <sup>g, h</sup>	297 <sup>h</sup>	$> 1.0 \times 10^4$ h	$\lesssim 0.1$ g, h	Early type <sup>i</sup>
A 1118-61	405	--	$4 \times 10^{-2} (D/2 \text{ kpc})^2$ j "	
4U1538-52	529	$> 10^3$ a	0.15 <sup>k</sup>	Early type
4U1223-62=GX 301-2	699	120	0.3	Early type
4U0352+30=X Per	835	$5.9 \times 10^3$	$4 \times 10^{-4}$	Early type

---

\* From Bradt et al., 1979, unless otherwise noted.

+ From Ghosh and Lamb, 1979, unless otherwise noted. In the column for  $L_x$ , D is the distance to the source.<sup>x</sup>  $L_x$  has been calculated by using the observed X-ray flux and estimated distance, taken from Ref (a) when given there.

a Bradt et al. 1979

b Rappaport et al. 1977

c Kelley et al. 1980

d White and Pravdo, 1979

e Armstrong et al. 1979

f Dower et al. 1978

g Lamb et al. 1980

h White et al. 1980

i Hutchings et al. 1980

j Ives et al. 1975

k Seward et al. 1976

100 s to 1000 s and only two in the range 10 s to 100 s. Thus the number of pulsars in the decade 10 s to 100 s is significantly less than their number in the lower ( $\sim 1$  s to 10 s) and the higher (100 s to 1000 s) decades.

2. Three of the slow pulsars ( $P > 100$  s) A0535 + 26, 4U1728-24 and 4U1223-62 have very small spin-up time scales  $T_s \lesssim 10^2$  years. Two of these have periods 104 s (A0535 + 26) and 116 s (4U 1728-24) at the lower end of the decade 100 s to 1000 s. At their present spin-up rate these pulsars can cross the gap 10 s - 100 s in just  $\lesssim 10^3$  years. The newly discovered 17.64 s X-ray pulsar also has a possible period derivative which is not inconsistent with a spin-up time scale  $T_s \sim 50$  years (Kelley et al., 1980). Period derivative for the 38.22 s X-ray pulsar is not known (White and Pravdo, 1979). Thus we see that X-ray pulsars with pulse period  $P$  in the range, 10 s to 100 s, and those which are entering this range from the top at  $P \sim 100$  s seem to cross the period decade 10 s - 100 s in a time less than one tenth



of their life time which is estimated to be  $\sim 10^4$  years (Savonije, 1980). Spin-up time scale  $T_s$  for the rest of the pulsars is comparable to their X-ray life-time  $\sim 10^4$  years.

In view of the above it is therefore suggested here that the gap in the pulse-period distribution, in the decade 10 s to 100 s is significant; not only because the population of pulsars in this period range is low, but also because the pulsars seem to rush through this period range on a time scale small compared to their life time. Below we discuss two processes which help maintain such a double-humped distribution of pulsar periods with a dip in the period-decade,  $\sim 10$  s to  $\sim 100$  s. It is shown that this gap is a result of the evolution of the rotation-rates of the magnetised neutron stars in the underlying binary systems. Mass transfer in these binary systems via a magnetosphere is accompanied by transport of angular momentum which makes the neutron star spin-rates to change.

### VI.3 Production and Maintenance of the Period Gap

#### I.3:1 SLOW-DOWN MECHANISM AND RELEVANT FORMULAE:

Several authors have discussed mechanisms to slow down the neutron star spin to long periods in mass-

transfer binary systems (Davidson and Ostriker, 1973 ; Illarionov and Sunyaev, 1975; Fabian, 1975; Kundt, 1976). First, the rotation of the young neutron star is slowed down by pulsar radiation and cosmic ray acceleration mechanism (Illarionov and Sunyaev, 1975). When the rotation period becomes greater than a critical period, matter captured by the neutron star from that lost by the normal companion penetrates the velocity of light cylinder. However, infall of the captured matter is arrested at the magnetopause where the magnetic pressure balances the effective gas pressure (see e.g. Pringle and Rees, 1972; Illarionov and Sunyaev, 1975). For a dipole magnetic field of a neutron star of mass  $M_x$ , radius  $R_x$ , surface magnetic field  $B_x$ , capturing matter at a rate  $\dot{M}_a$ , the radius of the magnetopause  $R_m$  is given by (See e.g. Vasyliunas, 1979)

$$R_m = 10^9 f_a \left( \frac{M_x}{M_\odot} \right)^{-1/7} \left( \frac{R_x}{10 \text{ km}} \right)^{12/7} \left( \frac{B_x}{3 \times 10^{12} \text{ Gauss}} \right)^{4/7} * \left( \frac{\dot{M}_a}{10^{-10} M_\odot / \text{yr}} \right)^{-2/7} \text{ cms,} \quad \text{VI. (1)}$$

where  $f_a \simeq 1$  for accretion from a stellar wind

$$\text{and } f_a = (\xi / \phi)^{2/7} \quad \text{for disc accretion from Roche-lobe overflow}$$

$$\text{with } \xi = \left( \frac{\text{average radial inflow speed in the disc}}{\text{free-fall speed}} \right)$$

$$\text{and } \phi = \left( \frac{\text{disc half-thickness}}{\text{radial distance}} \right)$$

Taking typical values for  $\xi$  and  $\phi$  in accretion discs,  
 $\xi = 1/100$ ,  $\phi = 1/20$  (e.g. Pringle and Rees, 1972)  
 we have

$$f_a \simeq 0.6 \text{ for disc accretion.}$$

At the magnetopause the accreting matter is forced into co-rotation with the neutron star magnetosphere. If the co-rotation speed ( $V_c = 2\pi R_m / P$ ) at the magnetopause exceeds the Keplerian orbital speed there ( $V_k = \sqrt{GM_x / R_m}$ ), matter is accelerated by the rotating magnetosphere and may be flung away, preventing accretion onto the neutron star. This results into a torque on the neutron star which slows down its spin (see e.g. Davidson and Ostriker, 1973). The co-rotation radius  $R_c$  where the co-rotation speed is equal to the Keplerian orbital speed, is given by

$$R_c = 1.5 \times 10^8 \left( \frac{M_x}{M_\odot} \right)^{1/3} \left( \frac{P}{1 \text{ s}} \right)^{2/3} \text{ cm} \quad \text{VI(2)}$$

Spin-down of the neutron star continues until  $R_m \leq R_c$ .

When this happens, matter can be accreted down to the neutron star. Accreting matter now brings angular momentum with it and this results in neutron star spin-up. Thus, at a given accretion rate, the accretion torques will bring the spin period  $P$  to a critical value  $P_c$  given by,

$$\begin{aligned} \left( \frac{P_c}{1 \text{ s}} \right) &= 17 f_a^{3/2} \left( \frac{M_x}{M_\odot} \right)^{-5/7} \left( \frac{R_x}{10 \text{ km}} \right)^{18/7} * \\ &* \left( \frac{B_x}{3 \times 10^{12} \text{ Gauss}} \right)^{6/7} \left( \frac{M_a}{10^{-10} M_\odot/\text{yr}} \right)^{-3/7} . \end{aligned} \quad \text{VI(3)}$$

at which  $R_m = R_c$ . This follows from Equations VI(1) and VI(2) with the condition  $R_m = R_c$ .

Also, at any given spin period  $P$ , if the accretion rate  $M_a$  increases beyond a critical value  $M_{ac}$  given by

$$\left( \frac{M_{ac}}{10^{-10} M_{\odot}/yr} \right) = 3.5 f_a \left( \frac{M_x}{M_{\odot}} \right)^{-5/3} \left( \frac{R_x}{10 \text{ km}} \right)^6$$

$$* \left( \frac{B_x}{3 \times 10^{12} \text{ Gauss}} \right)^2 \left( \frac{P}{100 \text{ s}} \right)^{-7/3}, \quad \text{VI(4)}$$

$R_m$  becomes less than  $R_c$  and material is accreted by the neutron star which turns into an X-ray pulsar with X-ray luminosity

$$L_x = 9 \times 10^{35} \left( \frac{M_x}{M_{\odot}} \right) \left( \frac{R_x}{10 \text{ km}} \right)^{-1}$$

$$* \left( \frac{M_a}{10^{-10} M_{\odot}/yr} \right) \text{ ergs sec}^{-1}, \quad \text{VI(5)}$$

energy being derived from the gravitational potential energy of the accreted material.

The neutron star spins up on a time scale  $T_s = -P/\dot{P}$  which for disc accretion is given by (Rappaport and Joss, 1977b)

$$T_s = - \frac{P}{\dot{P}} = 3 \times 10^4 f_s \left( \frac{P}{1 \text{ s}} \right)^{-1} \left( \frac{L_x}{10^{37} \text{ erg sec}^{-1}} \right)^{-6/7} \text{ years,}$$

VI(6)

where  $f_s$  is of order unity.

Having presented the relevant physical processes and the required formulae we now attempt to explain the shape of the pulse-period distribution of binary X-ray pulsars.

### VI.3:2 CHARACTER OF MASS TRANSFER AND THE PULSE-PERIOD DISTRIBUTION

From Table VI.1 we find that the optical companions of the binary X-ray pulsars are of two types. Low-mass stars and massive early-type stars. One pulsar (GX 1 + 4) has a late-type giant as its optical companion. As discussed above, after the initial slow-down by the conventional pulsar emission, material captured by the neutron star from that lost by the optical companion is rotationally ejected by the magnetosphere and the rotation period is brought to the value  $P_c$  which depends on the rate of capture of matter  $\dot{M}_a$  (see Equation VI(3)).

For accretion from a stellar wind from the normal star an estimate of  $M_a$  can be easily made. If the stellar wind mass loss rate from the normal star be  $M_1$  and wind velocity  $V_w$ , then for a neutron star of mass  $M_x$  at a binary orbital separation  $A$ , the rate of capture of mass  $M_a$  will be  $M_a = \frac{1}{4} \left( \frac{r_a}{A} \right)^2 M_1$  where  $r_a$  is the capture radius given by  $r_a = \frac{GM_x}{V_w^2}$ .

We obtain

$$M_a \simeq 4 \times 10^{-5} \left( \frac{M_x}{M_\odot} \right)^2 \left( \frac{A}{10^{12} \text{ cm}} \right)^{-2} \left( \frac{V_w}{1000 \text{ km sec}^{-1}} \right)^{-4} M_1.$$

VI(7)

We will now consider the slow-down of neutron stars in the two types of binary systems (Low mass and Massive) separately.

#### (i) LOW-MASS BINARY X-RAY PULSARS:

For X-ray pulsars in low mass binary systems, the mass loss from the normal star by stellar wind will be very weak. For such a system, if we take  $M_1 \sim 10^{-13} M_\odot/\text{yr}$ ,  $A \sim 10^{11} \text{ cm}$  and  $V_w \sim 1000 \text{ km/sec}$ , we get from Equation VI(7)

$\dot{M}_a \sim 4 \times 10^{-16} M_\odot/\text{yr}$ . A stellar wind so weak will take  $\sim 10^{11}$  years to penetrate the light cylinder (Illarionov and Sunyaev, 1975) and thus can not slow down the pulsar to the period  $P_c$ . However, as the normal star evolves, mass transfer by Roche-lobe overflow will become important in such systems. In this case, taking a typical value for  $\dot{M}_a \sim 10^{-10} M_\odot/\text{yr}$  (e.g. Faulkner, 1976) in Equation VI(3) we find that by disc accretion ( $f_a \simeq 0.6$ ), the neutron star in such systems can be slowed down to the period  $P_c \sim 8$  sec.

Thus X-ray pulsars in low mass binaries will have  $P \lesssim 10$  s and  $L_x \sim 10^{36}$  ergs/sec at the time of their X-ray turn on, and as the accretion rate increases, they will spin-up toward  $P \sim 1$  s with  $T_s \sim 10^4$  years and  $L_x \gtrsim 10^{36}$  erg/sec. This follows from Equations VI(3), VI(5) and VI(6). X-ray pulsars 4U 1627-67 (7.68 s) and Her X-1 (1.24 s) could be examples of such systems. In the pulse-period distribution such pulsars belong to the group with  $1 \text{ s} \lesssim P \lesssim 10 \text{ s}$ . They have probably never had  $P \gg 10$  s.

## (ii) MASSIVE BINARY X-RAY PULSARS:

When the optical companion of an X-ray pulsar is a massive early type star, mass loss by stellar wind from the normal star can be quite high. At the present time



(the phase after X-ray turn on) most of the X-ray pulsars in massive binaries seem to be disc-fed ( Rappaport and Joss, 1977 b; Ghosh and Lamb, 1979 ), but before the critical-lobe overflow begins, during the neutron star slow-down phase, mass loss from the normal early type star will be by means of a stellar wind. Adopting typical stellar wind parameters for the early type companion,  $\dot{M}_1 \sim 10^{-8.5} M_{\odot}/\text{yr}$  and  $V_w \sim 1000 \text{ km/sec}$  (Rogerson and Lamers, 1975; Snow and Marlborough, 1976) , from Equation VI(7) we get  $\dot{M}_a \sim 10^{-13} M_{\odot}/\text{yr}$  and with this value of the capture rate, we find from Equation VI(3) that a typical X-ray pulsar in such binary systems will be slowed down to the period  $P_c \sim 330 \text{ sec.}$

Thus it is clear that stellar winds from the early type star in massive binary systems can slow down the X-ray pulsars to the period range  $P \sim 100 \text{ s}$  to  $P \sim 1000 \text{ s.}$

From the above discussion, we find that at the time of X-ray turn-on an X-ray pulsar will belong either to the group of fast pulsars ( $1 \text{ s} \lesssim P \lesssim 10 \text{ s}$ ) or to the group of slow pulsars ( $100 \text{ s} \lesssim P \lesssim 1000 \text{ s}$ ), depending on whether the slow-down occurred by Roche-lobe overflow in a low-mass binary system or by stellar wind in a massive binary system.

After the X-ray turn-on the X-ray pulsars undergo a secular spin-up and a secular increase in luminosity  $L_x$  because of the evolution of the primary star overflowing its Roche-lobe (Savonije, 1978). Mass transfer in X-ray pulsars with early-type companions is taking place, at the present time, probably by means of atmospheric Roche-lobe overflow as suggested by Savonije (1979).

From Table VI.1 we find that the fast X-ray pulsars with early-type companions (SMC X-1, 4U 0115 + 63 and Cen X-3) and the slow pulsars which are spinning up on time scales  $T_s \lesssim 100$  years, have X-ray luminosities  $L_x \gtrsim 10^{37}$  erg/sec; whereas the rest of the slow pulsars have  $L_x \lesssim 10^{36}$  erg/sec and  $T_s \sim 10^4$  years. We therefore conclude that after the X-ray turn-on, so long as the mass transfer rate by atmospheric Roche-lobe overflow  $M_a \lesssim 10^{-10} M_\odot/\text{yr}$ , the slow X-ray pulsars remain in the period range  $P \gtrsim 100$  s and when the overflow rate picks up to  $M_a \gtrsim 10^{-9} M_\odot/\text{yr}$ , X-ray luminosity becomes  $L_x \gtrsim 10^{37}$  erg/sec and the pulsar spins up on a time scale  $T_s \sim 10^2$  years (as can be seen from Equation VI(6)). When this happens, the pulsar crosses the period range 100 s - 10 s in just about  $10^3$  years. As the increasing mass transfer rate reaches the value  $M_a \sim 10^{-8} M_\odot/\text{yr}$ , matter piles up around the X-ray source and the X-ray pulsar is extinguished (e.g., van den Heuvel, 1976).

#### VI.4 Conclusions

It thus appears that the gap in the pulse-period distribution of binary X-ray pulsars in the range from  $P \sim 10$  s to  $P \sim 100$  s is significant and is produced because neutron stars in these systems are slowed down, either to  $P \lesssim 10$  s by Roche-lobe mass transfer in low-mass binaries or to  $P \gtrsim 100$  s by stellar winds in massive binaries. The period gap is then maintained as the slow pulsars cross this gap in a time very short compared to their life time, because of the increase in mass transfer rate with the evolution of the normal star. In fact, a population statistics of the massive binary X-ray pulsars in the different period ranges would suggest that the atmospheric overflow transfers matter in massive X-ray binaries at a rate  $\lesssim 10^{-10} M_{\odot}/\text{yr}$  for a few times  $10^4$  years and the mass transfer rate increases to  $10^{-9} M_{\odot}/\text{yr}$  and more on a time scale  $\lesssim 10^3$  years probably as the photosphere of the early type star begins to overflow the Roche-lobe.

## REFERENCES

- Alfven, H. and Carlqvist, P.; 1978, *Astrophys. Space Sci.* 55, 487.
- Allen, C.W.; 1973, *Astrophysical Quantities*, Athlone Press, London.
- Armstrong, J.T., Johnston, M.D., Eradt, H.V., Cowley, A.P., Doxsey, R.E., Griffiths, R.E., Hesser, J.E. and Schwartz, D.A.; 1979, Preprint.
- Baines, M.J., Williams, I.P. and Asebiomo, A.S.; 1965, *Monthly Not. Roy. Astron. Soc.*, 130, 63.
- Barnard, E.E.; 1927, Carnegie Institution of Washington Publication No. 247, Part I.
- Bhattacharjee, S.K. and Williams, I.P.; 1980, *Astron. Astrophys.*, 91, 85.
- Bok, B.J.; 1977, *Publ. Astron. Soc. Pacific*, 89, 597.
- Bok, B.J. and McCarthy, C.C.; 1974, *Astron. J.*, 79, 42.
- Bok, B.J. and Reilly, E.J.; 1947, *Astrophys. J.*, 105, 255.
- Bradt, H.V., Doxsey, R.E. and Jernigan, J.C.; 1979, in W.A. Baity and L.E. Peterson (eds.), 'X-ray Astronomy,' COSPAR, Pergamon Press, Oxford, 3.
- Carrasco, L., Strom, S.E. and Strom, K.M.; 1973, *Astrophys. J.*, 182, 95.
- Clark, F.O. and Johnson, D.R.; 1982, *Astrophys. J.*, 263, 160.
- Cordova, F.A., Chester, T.J., Tuohy, I.R. and Garmire, C.P.; 1980, *Astrophys. J.*, 235, 163.

- Coyne, G., Gehrels, T. and Serkowski, K.; 1974, *Astron. J.*, 79, 581.
- Davidson, K. and Ostriker, J.P.; 1973, *Astrophys. J.*, 179, 585.
- Davis, L. Jr. and Greenstein, J.L.; 1951, *Astrophys. J.*, 114, 206.
- Dickman, R.L.; 1978, *Astrophys. J. Suppl.*, 37, 407.
- Dohnanyi, J.S.; 1969, *J. Geophys. Res.*, 74, 2531.
- Dower, R.G., Apparao, K.M.V., Bradt, H.V., Doherty, R.E. et al.; 1978, *Nature*, 273, 364.
- Fabian, A.C.; 1975, *Monthly Not. Roy. Astron. Soc.*, 173, 161.
- Faulkner, J.; 1976, in P. Eggleton, S. Mitton and J. Whelan (eds.), 'Structure and Evolution of Close Binary Systems,' IAU Symp. 73, D. Reidel Publ. Co., Dordrecht, 193.
- Field, G.B.; 1973, in M.A. Gordon and L.E. Snyder (eds.), 'Molecules in the Galactic Environment,' John Wiley and Sons, New York, 21.
- Field, G.B. and Saslaw, W.; 1965, *Astrophys. J.*, 142, 583.
- Fischer, J., Righini-Cohen, G., Simon, M. and Cassar, L.; 1979, *Astron. J.*, 84, 1574.
- Fowler, W.A. and Hoyle, F.; 1963, *R. Obs. Bull.*, No. 67, 301.
- Ghosh, P. and Lamb, F.K.; 1979, *Astrophys. J.*, 234, 296.
- Greenberg, J.M.; 1968, in B.M. Middlehurst and L.H. Aller (eds.), 'Nebulae and Interstellar Matter,' University of Chicago Press, 221.
- Hall, J.S.; 1949, *Science*, 109, 166.

- Handbury, M.J., Simons, S. and Williams, I.P.; 1977, *Astron. Astrophys.*, 61, 443..
- Hartmann, J.; 1904, *Astrophys. J.*, 19, 268.
- Hiltner, W.A.; 1949, *Science*, 109, 165.
- Hodge, P.W.; 1972, *Publ. Astron. Soc. Pacific*, 84, 365.
- Hodge, P.W.; 1974, *Publ. Astron. Soc. Pacific*, 86, 263.
- Hodge, P.W.; 1980, *Astron. J.*, 85, 376.
- Horedt, G.P.; 1973, *Monthly. Not. Roy. Astron. Soc.*, 163, 285.
- Horedt, G.P.; 1976, *Astrophys. Space Sci.*, 45, 353.
- Hughes, D.W. and Daniels, P.A.; 1980, *Monthly Not. Roy. Astron. Soc.*, 191, 511.
- Hutchings, J.B., Cowley, A.P. and Crampton, E.; 1980, *IAU Cir. No.3544*.
- Illarionov, A.F. and Sunyaev, R.A.; 1975, *Astron. Astrophys.*, 39, 185.
- Ives, J.C., Sanford, P.W. and Bell Burnell, S.J.; 1975, *Nature*, 254, 578.
- Jenkins, E.B. and Savage, D.B.; 1974, *Astrophys. J.*, 187, 243.
- Jones, T.J., Hyland, A.R., Robinson, G., Smith, R. and Thomas, J.; 1980, *Astrophys. J.*, 242, 132.
- Keene, J.; 1981, *Astrophys. J.*, 245, 115.
- Kelley, R.L., Apparao, K.M.V., Doxsey, R.E., Jernigan, J.G., Naranan, S. and Rappaport, S.; 1980, Preprint.

- Kenyon, S. and Starrfield, S.; 1979, Publ. Astron. Soc. Pacific, 91, 271.
- Khavtassi, J. Sh.; 1960, Atlas of Galactic Dark Nebulae, Abastumani Astrophysical Observatory.
- Kundt, W.; 1976, Phys. Letters, 57A, 195.
- Kushwaha, R.S. and Kothari, D.S.; 1960, Z. Astrophys., 51, 11.
- Lamb, R.C., Markert, T.H., Hartman, R.C., Thompson, D.J. and Bignami, G.F.; 1980, Astrophys. J., 239, 651.
- Larson, R.B.; 1969, Monthly Not. Roy. Astron. Soc., 145, 271.
- Lundmark, K. and Melotte, P.J.; 1926, Upsala Medd., No. 12.
- Lynds, B.T.; 1962, Astrophys. J. Suppl. 7, 1.
- Martin, R.N. and Barrett, A.H.; 1978, Astrophys. J. Suppl. 36, 1.
- McCrea, W.H. and Williams, I.P.; 1965, Proc. R. Soc., A287, 143.
- McMillan, R.S.; 1978, Astrophys. J., 225, 880.
- Milman, A.S.; 1977, Astrophys. J., 211, 128.
- Oort, J.H.; 1954, Bull. Astron. Inst. Neth., 12, 177.
- Penston, M.V.; 1969, Monthly Not. Roy. Astron. Soc., 144, 425.
- Penston, M.V., Munday, A., Stickland, D.J. and Penston, M.J.; 1969, Monthly Not. Roy. Astron. Soc., 142, 355.

- Pringle, J.E. and Rees, M.J.; 1972, *Astron. Astrophys.*, 21, 1.
- Rappaport, S.A., Markert, T., Li, F.K., Clark, G.W. et al.; 1977, *Astrophys. J. Lett.*, 217, L29.
- Rappaport, S.A. and Joss, P.C.; 1977a, *Nature*, 266, 123.
- Rappaport, S.A. and Joss, P.C.; 1977b, *Nature*, 266, 683.
- Reddish, V.C.; 1978, *Stellar Formation*, Pergamon Press.
- Rogerson, J.B. and Lamers, H.G.; 1975, *Nature*, 256, 190.
- Rowan-Robinson, M.; 1979, *Astrophys. J.*, 234, 111.
- Salpeter, E.E.; 1955, *Astrophys. J.*, 121, 161.
- Savonije, G.J.; 1978, *Astron. Astrophys.*, 62, 317.
- Savonije, G.J.; 1979, *Astron. Astrophys.*, 71, 352.
- Savonije, G.J.; 1980, *Astron. Astrophys.*, 81, 25.
- Schmidt, E.G.; 1975, *Monthly Not. Roy. Astron. Soc.*, 172, 401.
- Schoenberg, E.; 1964, *Veroffentl. Sternwerte Munchen*, 5, No. 21.
- Serkowski, K.; 1968, *Astrophys. J.*, 154, 115.
- Serkowski, K., Mathewson, D.S. and Ford, V.L.; 1975, *Astrophys. J.*, 196, 261.
- Seward, F.D., Page, C.G., Turner, M.J.L. et al., 1976, *Monthly Not. Roy. Astron. Soc.*, 177, 13p.



- Snell, R.L.; 1981, *Astrophys. J. Suppl.*, 45, 121.
- Snow, T.P. and Marlborough, J.M.; 1976, *Astrophys. J. Lett.*, 203, L87.
- Stebbins, J., Huffer, C.M. and Whitford, A.; 1940, *Astrophys. J.*, 91, 20.
- Strom, S.E., Strom, K.M. and Grasdalen, G.L.; 1975, *Ann. Rev. Astron. Astrophys.*, 13, 187.
- Tomita, Y., Saita, T. and Ohtani, H.; 1979, *Publ. Astron. Soc. Jap.*, 31, 407.
- Turnshek, D.A., Turnshek, D.E. and Craine, E.R.; 1980, *Astron. J.*, 85, 1638.
- Trumpler, R.J.; 1930, *Lick Obs. Bull.*, 14, 154, No. 420.
- van den Heuvel, E.P.J.; 1976, in P. Eggleton, S. Mitton and J. Whelan (eds.), 'Structure and Evolution of Close Binary Systems', *IAU Symp.* 73, D. Reidel Publ. Co., Dordrecht, 35.
- Vasyliunas, V.M.; 1979, *Space Sci., Rev.*, 24, 609.
- White, N.E. and Pravdo, S.H.; 1979, *Astrophys. J. Lett.*, 233, L121.
- White, N.E., Pravdo, S.H., Becker, R.H., Boldt, E.A., Holt, S.S. and Serlemitsos, P.J.; 1980, *Astrophys. J.*, 239, 655.
- Wickramasinghe, N.C.; 1967, *Interstellar Grains*, Chapman and Hall, London.
- Williams, I.P.; 1972, in H. Reeves (ed.), 'Origin of the Solar System', C.N.R.S.

Williams, I.P. and Bhatt, H.C.; 1982, Monthly Not.  
Roy. Astron. Soc., 199, 465.

Williams, I.P. and Crampin, D.J.; 1971, Monthly Not. Roy.  
Astron. Soc., 152, 261.

Williams, I.P. and Handbury, M.J.; 1974, Astrophys. Space  
Sci., 30, 215.